

***Limulus polyphemus* Hemocyanin: 10 Å Cryo-EM Structure, Sequence Analysis, Molecular Modelling and Rigid-body Fitting Reveal the Interfaces Between the Eight Hexamers**

**Andreas G. Martin¹, Frank Depoix¹, Michael Stohr¹, Ulrich Meissner¹
Silke Hagner-Holler¹, Kada Hammouti¹, Thorsten Burmester¹
Jochen Heyd², Willy Wriggers² and Jürgen Markl^{1*}**

¹*Institute of Zoology, Johannes Gutenberg University D-55099 Mainz, Germany*

²*School of Health Information Sciences, University of Texas Health Science Center at Houston, Houston, TX 77030 USA*

The blue copper protein hemocyanin from the horseshoe crab *Limulus polyphemus* is among the largest respiratory proteins found in nature (3.5 MDa) and exhibits a highly cooperative oxygen binding. Its 48 subunits are arranged as eight hexamers (1×6mers) that form the native 8×6mer in a nested hierarchy of 2×6mers and 4×6mers. This quaternary structure is established by eight subunit types (termed I, IIA, II, IIIA, IIIB, IV, V, and VI), of which only type II has been sequenced. Crystal structures of the 1×6mer are available, but for the 8×6mer only a 40 Å 3D reconstruction exists. Consequently, the structural parameters of the 8×6mer are not firmly established, and the molecular interfaces between the eight hexamers are still to be defined. This, however, is crucial for understanding how allosteric transitions are mediated between the different levels of hierarchy. Here, we show the 10 Å structure (FSC_{1/2-bit} criterion) of the oxygenated 8×6mer from cryo-electron microscopy (cryo-EM) and single-particle analysis. Moreover, we show its molecular model as obtained by DNA sequencing of subunits II, IIIA, IV and VI, and molecular modelling and rigid-body fitting of all subunit types. Remarkably, the latter enabled us to improve the resolution of the cryo-EM structure from 11 Å to the final 10 Å. The 10 Å structure allows firm assessment of various structural parameters of the 8×6mer, the 4×6mer and the 2×6mer, and reveals a total of 46 inter-hexamer bridges. These group as 11 types of interface: four at the 2×6mer level (II–II, II–IV, V–VI, IV–VI), three form the 4×6mer (V–V, V–VI, VI–IIIB/IV/V), and four are required to assemble the 8×6mer (IIIA–IIIA, IIIA–IIIB, II–IV, IV–IV). The molecular model shows the amino acid residues involved, and reveals that several of the interfaces are intriguingly histidine-rich and likely to transfer allosteric signals between the different levels of the nested hierarchy.

© 2006 Elsevier Ltd. All rights reserved.

Keywords: hemocyanin; cryo-electron microscopy; 3D reconstruction; quaternary structure; amino acid sequence

*Corresponding author

Present address: T. Burmester, Institute of Animal Physiology, Biocenter Grindel, University of Hamburg, D-20146 Hamburg, Germany.

Abbreviations used: SAXS, small angle X-ray scattering; MRA, multiple reference alignment; MSA, multivariate statistical analysis; FSC, Fourier shell correlation; EM, electron microscope.

E-mail address of the corresponding author:
markl@uni-mainz.de

Introduction

Arthropod hemocyanins are extracellular oxygen-transport proteins that exhibit a complex allosteric behaviour during oxygen binding, with Hill coefficients up to 9 in some Chelicerata, such as the horseshoe crab *Limulus polyphemus*. The oxygen-binding site of hemocyanin is formed by two copper ions that are directly bound to the protein, causing the blue colour of blood in the oxygenated state.^{1,2} A

very different hemocyanin family occurs in the phylum Mollusca; however, these are not considered here.³

Arthropod hemocyanins are hexamers (1×6mers) or oligohexamers (n ×6mers) of bean-shaped 75 kDa polypeptide subunits (~650 amino acid residues). The 3.2 Å resolution crystal structure of the deoxygenated 1×6mer of the spiny lobster (*Panulirus interruptus*) hemocyanin is known.⁴ The crystal structures of the deoxygenated and oxygenated subunit II of *L. polyphemus* hemocyanin became available at 2.4 Å resolution,^{5,6} and 1×6mers of subunit II have the same quaternary structure as the native 1×6mer of *Panulirus* hemocyanin.⁷ The subunit comprises three structural domains: The N-terminal domain 1 is rich in α -helices, the central domain 2 contains a four-helix bundle with the copper active site, and the C-terminal domain 3 is rich in β -sheets. Each structural domain plays a specific functional role.⁸ To build the hexamer, the six subunits are arranged as two trimers in D3 point-group symmetry. As deduced from sequence analysis of hemocyanin subunits from very distantly related arthropods, the secondary structure elements are highly conserved;^{9,10} therefore, the published crystal structures are likely to hold true for arthropod hemocyanin subunits in general.¹¹

Some arthropods, notably spiny lobsters such as *P. interruptus*, possess a hemocyanin that is a single hexamer. Also, the various copper-free hemocyanin homologues ("storage proteins") that occur in the hemolymph of many crustaceans and insects are single hexamers.¹² Other arthropods, such as the brachyuran crab *Carcinus maenas* or the ctenid spider *Cupiennius salei*, possess 2×6mer hemocyanin.¹³ A tetrahedral 4×6mer hemocyanin occurs in thalassinid shrimps, and a different 4×6mer is typical for many arachnids, such as tarantulas and scorpions.¹⁴ A peculiar 6×6-mer hemocyanin has been detected in scutigermorph centipedes.¹⁵ The largest arthropod hemocyanin known is the 8×6mer of horseshoe crabs, and has been particularly well studied in *L. polyphemus*. It shows cooperative oxygen binding and heterotropic allosteric regulation by protons, chloride ions and divalent cations,¹⁶ and its quaternary structure is stabilized by hydrophilic and polar forces.¹⁷ As deduced from immunoelectron microscopy and biochemical analyses, this 8×6mer consists of two arachnid-type 4×6mers assembled face-to-face.¹⁸

Whereas 1×6mer hemocyanin can be built from a single subunit type, the 2×6mers require at least two subunit types, with the second type forming the inter-hexamer bridge.¹³ In the chelicerate 4×6mer hemocyanins, seven or eight different subunits are required; they follow a fixed stoichiometry and occupy defined positions within the molecule. This heterogeneity has been correlated with the specific oxygen-binding properties of the respiratory protein and as prerequisite for the assembly beyond the hexamer.^{1,2,14} In *L. polyphemus* hemocyanin, eight different subunit types are present with a different number of copies: six of type I; two of type IIA; eight

of types II, IIIA, IIIB, and IV; and four of types V and VI.^{19,20} Immunological correlations of these subunits with the subunit complements of the scorpion *Androctonus australis* and the tarantula *Eurypelma californicum* are available,^{21,22} and the topological position of each subunit type within the 4×6mers of these three hemocyanins is known from immunoelectron microscopy.^{20,23–26} That each subunit type indeed fulfils a specific role in the oligomeric architecture has been confirmed by reassembly and hybrid reassembly experiments.^{20,27,28}

Although a plethora of arthropod hemocyanin subunit sequences are known,^{9,10} the complete subunit set of a particular hemocyanin has been sequenced in only a few cases. Among the chelicerates, this is the case for the tarantula *E. californicum*, the golden orb web spider *Nephila inaurata* (with one type missing) and the ctenid spider *Cupiennius salei*.^{29–31}

Thus, many details of the primary and quaternary structure of arthropod hemocyanins are known. However, sequence data of several functionally well-studied hemocyanins are incomplete or lacking, and the exact mode of the higher-ordered assembly of hexamers remains obscure. With respect to the 4×6mer/8×6mer chelicerate hemocyanins, different image analysis procedures were used to solve the quaternary structure of *Androctonus*, *Eurypelma* and *Limulus* hemocyanins, starting from electron microscope images of negatively stained preparations.^{18,32–35} In a different approach, using small-angle X-ray scattering (SAXS), structural differences between the oxy and the deoxy state of *Eurypelma* hemocyanin have been claimed.³⁶ A 3D reconstruction from cryo-electron microscope images was performed for the *Androctonus* 4×6mer,³⁷ and the *Limulus* 8×6mer,³⁸ but the resolution limit was about 40 Å in both cases. These approaches revealed various basic parameters of the 4×6mer and the 8×6mer, but a reliable molecular fitting of the crystal structure was not possible due to the low resolution obtained.

Previously, we presented a cryo-EM structure of *Palinurus elephas* (spiny lobster) hemocyanin below 10 Å, solved by single-particle analysis (8 Å according to the Fourier shell correlation (FSC)_{3 σ} criterion; 10 Å according to the FSC_{1/2-bit} criterion). This 3D reconstruction allowed a convincing fit with the crystal structure of *Panulirus interruptus* 1×6mer, and molecular modelling of some parts.³⁹ This result encouraged us to study, by cryo-EM, the 8×6mer hemocyanin of *L. polyphemus*.

Results and Discussion

3D cryo-electron microscopy

A total of 58 focal pair cryo-electron micrographs (Figure 1) were recorded under low-dose conditions, and image analysis was performed as described in Materials and Methods. The resulting 3D reconstruction was calculated with 11,633 single particles

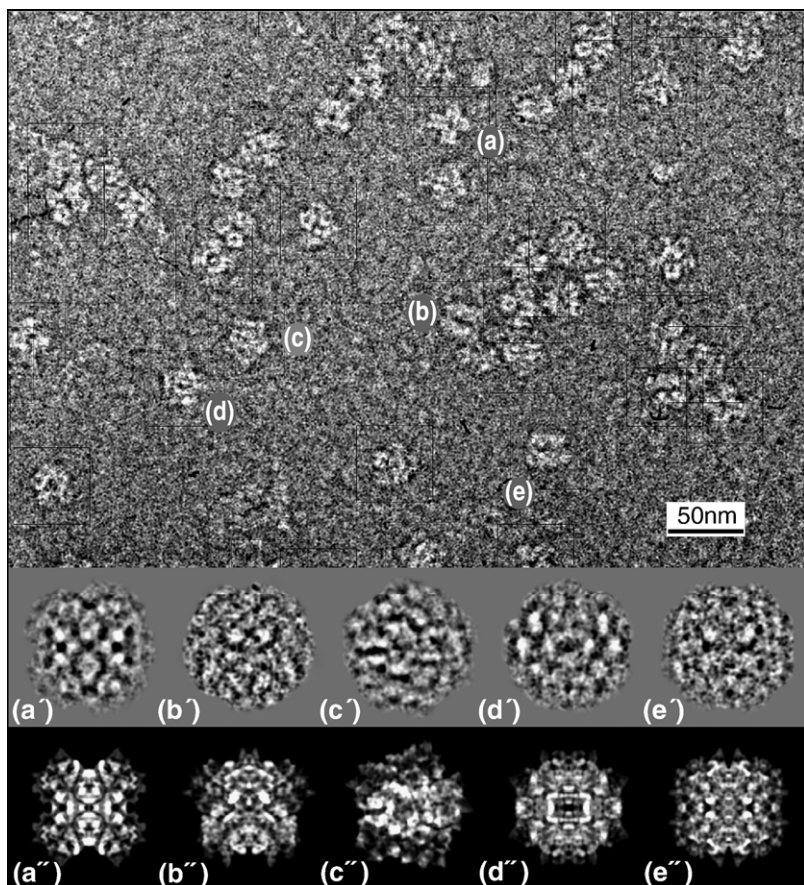


Figure 1. Cryo-electron microscopy and image processing of the *Limulus* hemocyanin 8×6mer. (a)–(e) The 8×6mer particles on a low-pass filtered cryo-electron micrograph, visible in (a) cross-view, (b) bow-tie view, (c) symmetric pentagonal view, (d) ring view, and (e) lateral view.³⁸ (a')–(e') Gallery of five different final class averages showing the same views as above. The class averages are high-pass filtered to stress high-frequency structural details and thus appear fuzzier than the particles in the micrograph. (a'')–(e'') Gallery of the corresponding reprojections.

averaged in 766 classes and achieved a resolution of 10.8 Å (FSC_{1/2-bit} criterion) and 8.8 Å (FSC_{3σ} criterion). This reconstruction (not shown) was used for the molecular fitting as described below and in Materials and Methods. The resulting molecular model of the whole 8×6mer was converted into a density map, low-pass filtered to a nominal 5 Å and used as a reference for the final refinement round, applying projection matching. The final cryo-EM structure was calculated with the whole data set (12,069 single particles) in 1140 class averages (~11 particles per class). Examples of these classes and their reprojections are presented in Figure 1.

As shown in Figure 2(a), the FSC curve crosses the FSC_{1/2-bit} noise curve at 9.6 Å and the FSC_{3σ} noise curve at 8.1 Å, whereas the FSC_{0.5} cut-off is at 12.2 Å. Assuming 0.844 Da/Å³, the threshold was set at 0.01, corresponding to a molecular mass of ~3.5×10⁶ Da (48 subunits of 73,000 Da each). The resolution of the final cryo-EM structure of the 8×6mer is almost the same as in our previous 3D reconstruction of the native 1×6mer hemocyanin from *P. elephas*.³⁹ Indeed, the eight hexamers are clearly defined and exhibit molecular detail; notably, the 48 individual subunits are discernible (Figure 3(a)–(c)). The handedness of the 1×6mer was confirmed by X-ray analysis of *P. interruptus* hemocyanin crystals;⁴ this allowed unambiguous assignment of the correct handedness to the cryo-EM density map of the 8×6mer.³⁴

The topology of the eight subunit types of the *Limulus* hemocyanin 8×6mer is known.²⁰ This allowed us to identify, in the present 10 Å cryo-EM structure, the individual subunits types and to label them with their correct designations (Figure 3(a')–(c')). In the case of subunit types I, II, IIIA, IIIB and IV that each occur in each hexamer as a single copy, this assignment was clearly defined. The sixth position in each hexamer is occupied by subunit V or subunit VI. These two subunits form a central heterodimeric bridge within the basic 2×6mer and a central tetrameric ring within the 4×6mer (see Figure 3(c')). This leaves two possibilities for their orientation: that shown in Figure 3(c'), or the alternative one with the labels V and VI exchanged. In the case of subunit I, the picture is complicated because in two hexamers this subunit type is substituted for a structural variant termed subunit IIA;²⁰ this subunit is incorporated in Figure 3(a')–(c') but is of no relevance for the present study, because within the *Limulus* 8×6mer, subunits I/IIA occupy the outer edges of the eight hexamers and are not involved in any inter-hexamer contact (see Table 2). The known subunit topology of the 8×6mer provided us with a firm basis for molecular fitting (see below).

Architecture of the 8×6mer

The architecture of the 8×6mer has been described.^{20,32–34,38,40} It consists of two identical

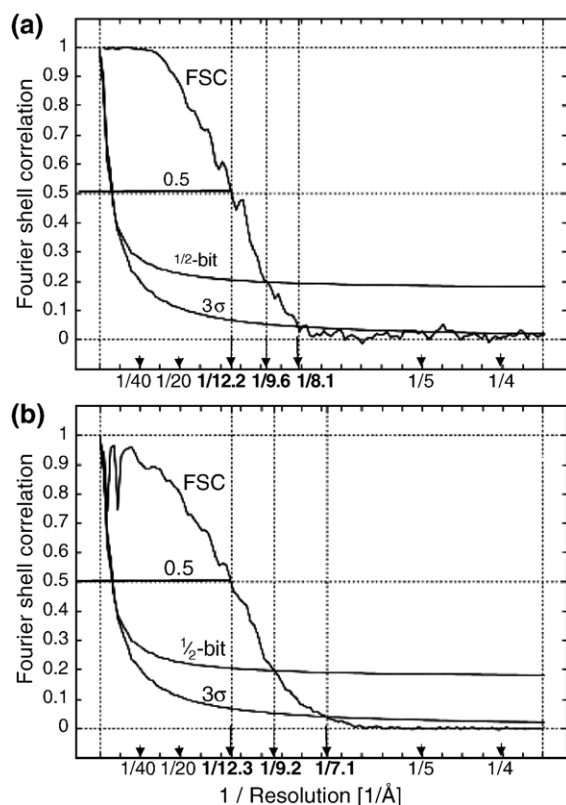


Figure 2. Resolution determination by Fourier shell correlation (FSC). (a) Resolution of the final cryo-EM 3D reconstruction. In this study, the resolution of the 3D reconstruction is defined by the $FSC_{1/2\text{-bit}}$ criterion; it is the reciprocal value of the spatial frequency at the intersection point of the FSC curve with the $FSC_{1/2\text{-bit}}$ noise curve (upper hyperbola). The previously applied $FSC_{3\sigma}$ criterion (calculated from the $FSC_{3\sigma}$ noise curve; lower hyperbola) yields values that are considered to be rather too optimistic. In contrast, the classical $FSC_{0.5}$ criterion (continuous horizontal line) yields values that are considered to be too pessimistic. (b) FSC of the final cryo-EM structure against the 3D volume of the molecular model used as reference in the final projection matching step. Note that the obtained values for the three FSC criteria are similar to the values in (a).

4×6mers that correspond structurally to the native 4×6mer hemocyanins of some arachnids, such as *E. californicum* and *A. australis*. The 4×6mer is assembled from two identical 2×6mers (dodecamers) lying side by side in an antiparallel orientation, but shifted and skewed significantly with respect to each other. Within each 2×6mer, the two 1×6mers (hexamers) are rotated $\sim 105^\circ$ with respect to each other; they differ slightly in their subunit composition (see Figure 3(a')). Because of the D2 point-group symmetry of the 8×6mer structure, a repeating 2×6mer is the basic building block of the 3D reconstruction. Some previously published parameters of 4×6mer and 8×6mer hemocyanins are summarized in Table 1, together with the values obtained in the present study.

The most detailed 3D reconstruction of an 8×6mer previously published has a resolution of ~ 40 Å.³⁸

Compared to this, the present 10 Å structure allows, with superior accuracy, the assignment of the different positions, shifts and rotations of the two hexamers within the basic 2×6mer, and of the four 2×6mers within the whole molecule. Measurements were performed by two different approaches. First, densities of 1×6mers, 2×6mers, and 4×6mers were extracted from the total density map, and volume alignments were calculated. Second, the generated and fitted models were aligned against each other. The measurements were assessed within the Resol-verT software package and yielded the following results (see also Table 1):

The basic 1x6mer

The hexamer is composed of two staggered layers of three bean-shaped subunits (staggering angle 120° ; D3 point-group symmetry). It appears as a hexagon when viewed from the top (along its 3-fold axis) and as a square when viewed from the side (see Figure 4(a)). Although the crystal structures of a native crustacean hemocyanin hexamer and of a hexamer assembled from subunit II of *Limulus* hemocyanin are available, and show the shape and arrangement of the six subunits at high resolution,^{4,5} and, significantly, yielded a perfect fit with our recent 10 Å cryo-EM structure of a native 1×6mer,³⁹ it cannot be *a priori* taken for granted that this arrangement is copied exactly in the various higher-order assemblies. Indeed, a slight but significant deformation was observed by molecular fitting of the subunit II homo-hexamers crystal structure and the present cryo-EM density map (see below). The degree of this twisting depends on the subunit position within the whole molecule and the contacts with subunits in neighbouring hexamers. Therefore, this is not a reconstruction artefact, but a consequence of the structural interactions between the eight hexamers. For the determination of parameters of the different hierarchy levels of *Limulus* hemocyanin, and interpretations of inter-hexamers interfaces, it is therefore crucial to deal with a density map determined from the whole 8×6mer,³⁸ instead of a map determined from a combination of sub-structures.^{35,36}

Parameters of the 2x6mer

In the 10 Å structure, the 2×6mer measures 146 Å (x -axis) \times 230 Å (y -axis) \times 168 Å (z -axis), and the local 3-fold axes of the constituent hexamers are $100(\pm 3)$ Å apart. With respect to the lower hexamer, the upper one shows three rotations: counterclockwise $8(\pm 2)^\circ$ around its local 3-fold axis, counterclockwise $105(\pm 5)^\circ$ around the dodecamer longitudinal axis, and 7° towards the observer (Figure 4(a); Table 1). This yields a close contact between the two hexamers and explains why biochemically isolated *Limulus* 2×6mers appear in the electron microscope as a combination of a hexagon and a square (e.g. see Figure 1b of Bijlholt *et al.*⁴⁰). Note that the 7° rotation is indeed $7+180^\circ$, which brings the two hexamers into an antiparallel position with respect to their subunit topology.

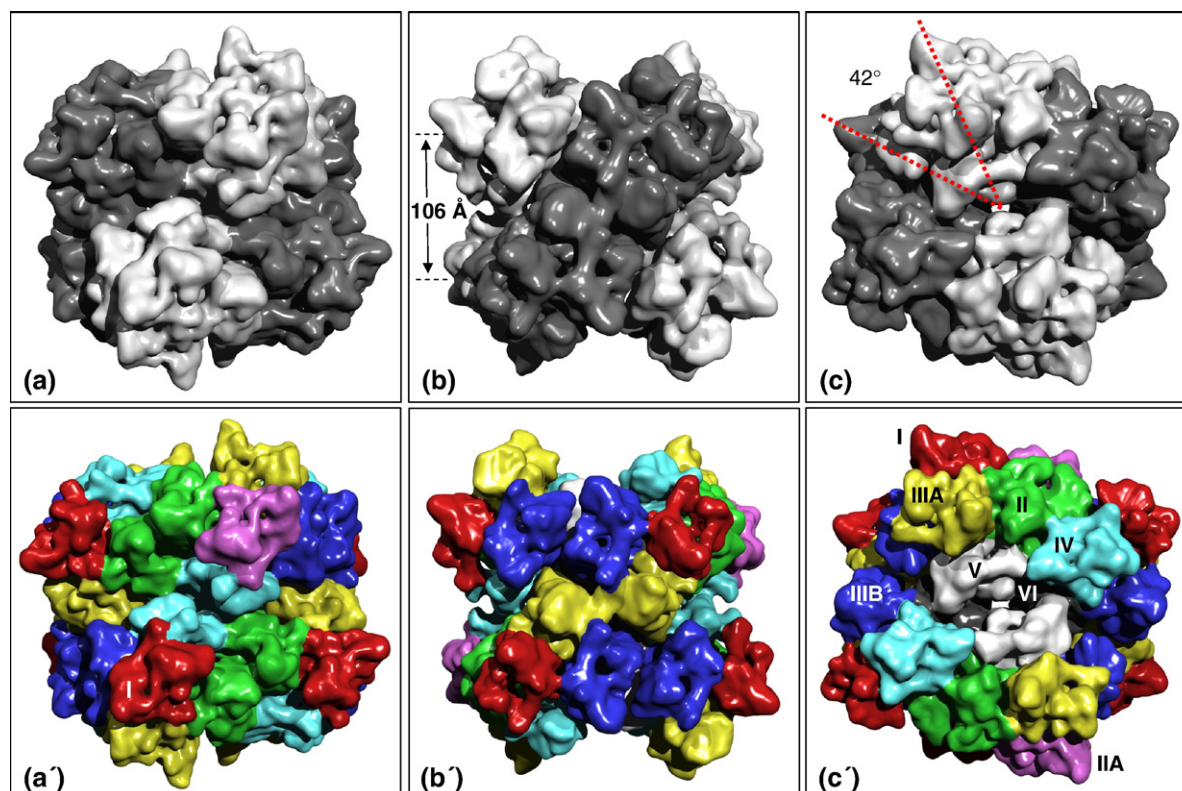


Figure 3. Views of the 3D reconstructed 8x6mer. (a) and (a') Lateral view (along the x -axis). (b) and (b') Cross-view (along the y -axis), with the distance of the two 4x6mers indicated. (c) and (c') Ring view (along the z -axis), with the staggering angle between the two 4x6mers indicated. In (a)–(c), the two hexamers within each 2x6mer are highlighted by light grey and anthracite, respectively. In (a')–(c'), the eight subunit types as biochemically defined,¹⁹ and topologically localized,²⁰ are indicated by different colours (red, type I; pink, type IIA; green, type II; yellow, type IIIA; blue, type IIIB; turquoise, type IV; white, type V; black, type VI). Note in (b) and (b') the prominent, oblique IIIA–IIIA bridge between the two associated 4x6mers (for molecular details, see Figure 10(a) and (a')). Note that in (c) and (c'), the flop face of the upper 4x6mer is visible (for comparison, see Figure 4(b) and (b')).

Parameters of the 4x6mer, flip-flop shift, and rocking effect

Within the 4x6mer half-molecule, which measures 249 Å (x -axis) × 244 Å (y -axis) × 168 Å (z -axis), the two 2x6mers are associated in an antiparallel arrangement, thereby showing a local 2-fold symmetry (Figure 4(b)–(e)). Their axial distance is 102(±3) Å, and the constituent 2x6mers are shifted 14(±1) Å

with respect to each other (see Figure 4(b) and (b')); and Table 1). This so-called flip-flop shift gives the 4x6mer, when viewed from the top, the shape of a parallelogram.³² As a consequence, two different top views are possible, depending on which face of the molecule is exposed to the observer when the 4x6mer rests on a support (see Figure 4(b) and (b')). These two orientations have been termed flip view and flop view, and define the two surfaces of the

Table 1. Structural parameters of the 4x6mer and 8x6mer hemocyanins

Molecule	Data	1x6mers in 2x6mer		2x6mers in 4x6mer			4x6mers in 8x6mer		Reference
		Distance (Å)	Rotation (°)	Distance (Å)	Flip-flop shift (Å)	Rocking angle (°)	Distance (Å)	Staggering angle (°)	
4x6mer ^a	3D (40 Å)	-	105	-	11	14	-	-	37
4x6mer ^b	2D	-	120	-	5	5±1	-	-	35
4x6mer ^b	SAXS _{oxy}	105±1.3	105±7	104.4±1.2	18±3	19±4	-	-	36
4x6mer ^b	SAXS _{deoxy}	104.5±0.8	131±3	103.5±0.8	4±2	6±3	-	-	36
8x6mer ^c	2D	102±5	90	108±5	17±4	12±3	102±5	32	34
8x6mer ^c	3D (40 Å)	-	103±2	-	12.8±3	12.5±3	108	40	38
8x6mer ^c	3D (10 Å)	100±3	105±5	102±3	14±1	16±2.5	106±3	42±2	This work

^a *Androctonus hemocyanin*.

^b *Eurytelma hemocyanin*.

^c *Limulus hemocyanin*.

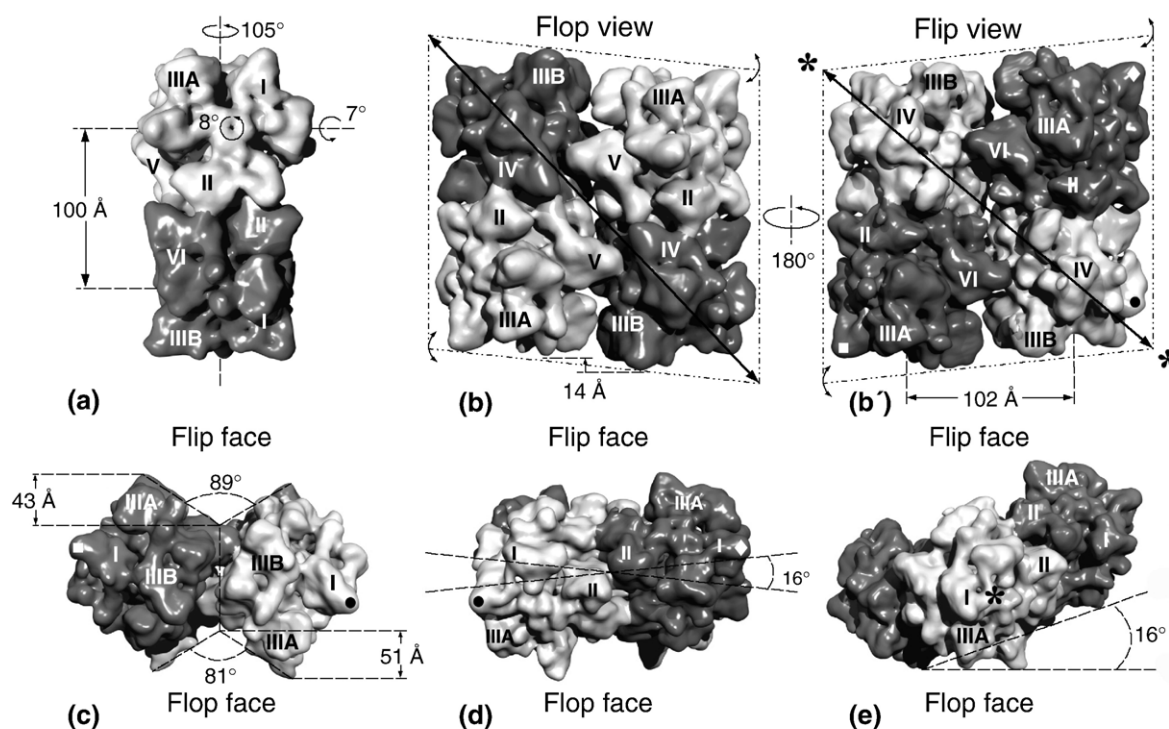


Figure 4. Parameters of the extracted 2×6mer and 4×6mer. (a) The 2×6mer, with the distance of the two hexamers, and the rotation of the upper hexamer around its longitudinal axis and around its 3-fold axis indicated. In addition, the 3-fold axis of the upper hexamer is tilted towards the observer, as marked. (b) Flop view of the 4×6mer (exposing its flop face to the observer), with the parallelogram-shape (broken line), the rocking axis (long diagonal) and the flip-flop shift indicated. Note that the lower 2×6mer is on the right (the long diagonal of the parallelogram runs from lower right to upper left). (b') Flip view of the 4×6mer (exposing its flip face to the observer), with the parallelogram-shape (broken line), the rocking axis (short diagonal; asterisks), and the distance of the 2×6mers indicated. Note that the lower 2×6mer is on the left (longer diagonal from lower left to upper right). (c) The 4×6mer viewed along the *y*-axis (i.e. along the V-shaped clefts between the 2×6mers), with the parameters of the clefts indicated. (d) The 4×6mer viewed along the *x*-axis, with the rocking angle indicated. In the flop view, rocking occurs around the long diagonal axis, and in the flip view around the short diagonal axis (see Figure 4(b) and (b')). (e) The 4×6mer viewed along the rocking axis (asterisk) of the flip view, with the rocking angle indicated. In (b'), (c) and (d), three types of small labels mark the corners to facilitate orientation. Note that there is confusion in the literature concerning the terms “flip face” and “flop face”,³⁸ we follow the terminology used by van Heel & Dube.³⁴

molecule as flip face and flop face.^{32,34} Each face shows a V-shaped longitudinal cleft that separates the two assembled 2×6mers; the two clefts differ in their contours (see Figure 4(c)).

The four hexamers are not coplanar, but the longitudinal axes of the 2×6mers are skewed with respect to each other by the so-called rocking angle (see Figure 4(d)). In the 10 Å structure, this rocking angle is 16(±2.5)°, which is comparable to published values (see Table 1). The rocking angle is responsible for the rocking behaviour of the 4×6mer.³² Due to the non-coplanar nature of the 4×6mer, only three of the four hexamers have contact to a plane support. To change between the two stable positions, the molecule has to rock on this support around a diagonal “rocking axis”. The resulting tilt angle of the 4×6mer (and the 8×6mer) between the two stable positions is the rocking angle (Figure 4(e)).

Parameters of the 8×6mer

In the 10 Å structure, the 8×6mer measures 284 Å (*x*-axis)×271 Å (*y*-axis)×282 Å (*z*-axis). The two

4×6mers have an axial distance of 106(±3) Å and are clearly assembled flip-to-flip, thereby exposing their flop faces; their staggering angle is 42(±2)° (see Figures 3(b) and (c) and 7(c)). Other workers have collected evidence for a flip-to-flip assembly,^{34,38} and predicted similar shifts and staggering angles (see Table 1). In the electron microscope, associations of two or more 8×6mers (flop-to-flop assembly), or of additional 4×6mers to the native 8×6mer (flop-to-flop or flip-to-flop assembly) are not observed; they would require molecular interfaces that apparently do not exist.

Primary structure and modelling of *Limulus* hemocyanin subunits

Sequence analysis

A cDNA library was constructed from the inner organs of a single adult specimen of *L. polyphemus*. This library was screened with two distinct polyclonal antibodies that were raised in rabbits against total *Limulus* hemocyanin. More than 100 positive

clones were identified, of which about 40 contained inserts that encode hemocyanin subunit cDNA. The hemocyanin sequences were assembled and completed by primer walking. On the basis of known N-terminal sequences,²⁰ the sequences were assigned to subunit types II, IIIA, IV and VI. The cDNA sequences have been deposited in the EMBL/ GeneBank database (see Materials and Methods). The primary structure of subunit II was already known from protein sequence analysis.¹¹

The cDNA sequences comprise 2054–2252 bp, which include 28 to 50 bp of the 5' untranslated regions and open reading frames of 1875–1917 bp. The 3' untranslated regions comprise 118–294 bp, include the standard polyadenylation signals (AATAAA) and are followed by poly(A) tails of variable lengths. The open reading frames of the hemocyanin subunits translate into distinct polypeptides of 624–638 amino acid residues (Figure 5),

with calculated molecular masses in the range of about 72–73.5 kDa. As in other chelicerate hemocyanins,^{29–31} no signal peptide required for transmembrane transport has been found in the *Limulus* subunit sequences. Thus, the nascent proteins do not pass through the Golgi apparatus, and the putative N-glycosylation sites (NXT/S) in the primary structures are probably not used.

Sequence comparison and phylogenetic tree

A multiple alignment of chelicerate hemocyanin amino acid sequences was constructed (available from the authors on request). Comparisons of the *Limulus* hemocyanin sequences with those of the arachnids *E. californicum*²⁹ and *N. inaurata*³¹ allowed an unambiguous and specific assignment of most, but not all, distinct subunit types. In phylogenetic analyses, which were carried out by Bayesian

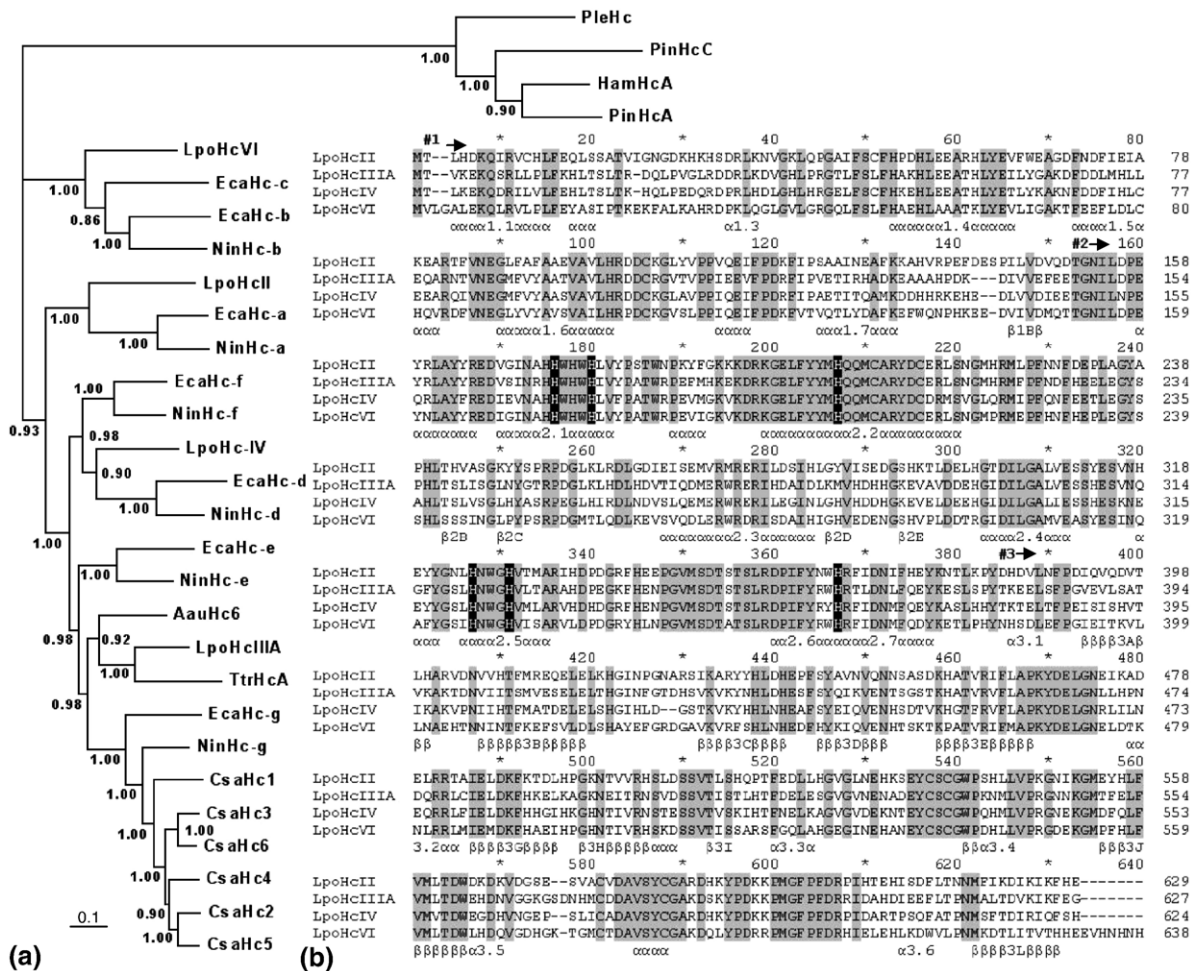


Figure 5. Sequence analysis of *Limulus* hemocyanin subunits. (a) Phylogeny tree of chelicerate hemocyanin subunits. The numbers at the nodes represent Bayesian posterior probabilities estimated with the WAG model of amino acid substitution. Species abbreviations are: Aau, *Androctonus australis*; Csa, *Cupiennius salei*; Eca, *Eurypelma californicum*; Lpo, *Limulus polyphemus*; Nin, *Nefila inaurata* and Ttr, *Tachypleus tridentatus* for the chelicerates; Ham, *Homarus americanus*; Ple, *Pacifastacus leniusculus*; Pin, *Panulirus interruptus* for the crustaceans (outgroup). (b) Alignment of the amino acid sequences of *L. polyphemus* hemocyanin subunits. Strictly conserved amino acids are shaded in grey, the Cu-binding histidine residues in black; the secondary structure elements as deduced from the X-ray structure of subunit II are indicated at the bottom.^{4–6} Note that the N-terminal methionine residue is not present in the secreted protein, as deduced from N-terminal protein sequencing.²⁰ #1, Domain 1; #2, domain 2; #3, domain 3

Table 2. Topological correspondencies of subunit types

Subunit type		Contribution to interfaces		
<i>Limulus</i>	<i>Eurypelma</i>	2×6mer	4×6mer	8×6mer ^a
I ^b , IIA ^b	e ^c	–	–	–
II ^c	a ^c	+	–	+
III ^a	g ^c	–	–	+
IIIB ^b	f ^c	–	+	+
IV ^c	d ^c	+	+	+
V ^b /VI ^c	b ^c /c ^c	+	+	–

^a Exclusively in *Limulus*.
^b Complete amino acid sequence is not available.
^c Complete amino acid sequence is available.

inference on the basis of the WAG model of amino acid substitutions, *Limulus* hemocyanin subunit II groups with the a-type subunits of the spiders, IIIA with the g-type subunits, IV with the d-type subunits and VI with the b/c-type subunits (see Figure 5). This assignment (Table 2) fits the results previously derived from immunochemical and reassembly studies.¹

Molecular modelling and rigid-body fitting

Because of the high degree of sequence similarity (>75%) between chelicerate hemocyanin subunits (see Figure 5), ternary structure modelling was straightforward on the basis of the published crystal structure of oxygenated subunit II.⁶ For modelling of the subunits IIIA, IV and VI, their authentic sequences were applied. Because the sequences of subunits I, IIA, IIIB and V are not known, structurally equivalent subunit sequences were used for modelling. In the case of subunit V, the

sequence of subunit VI was taken. In the case of subunits I, IIA and IIIB, the orthologous sequences of *Eurypelma* hemocyanin were applied (see Table 2). This is uncritical in the case of subunits I and IIA, because these subunit types (which play equivalent roles in the oligomeric architecture) are not involved in any inter-hexamer contact (see Table 3). In the case of subunits V and IIIB, however, these circumstances should be kept in mind. Also, the complete sequence of the subunit II was modelled for fitting into the density map of the cryo-EM structure. The amino acid residues 22–29, 134–138, 527–530 and 569–572, which are missing from the published crystal structure of *Limulus* subunit II, were modelled by means of spatial restraints.

The fitting procedure as described in Material and Methods resulted in a molecular model of the entire 8×6mer (Figure 6). Its quality was assessed by FSC (Figure 2(b)), and by calculating standard and Laplacian cross-correlations against the 10 Å cryo-EM structure, which yielded values of 0.810 and 0.802, respectively. Most of the amino acid residues in the molecular model of the 8×6mer do not overlap. Although a few side-chains overlap in some inter-hexamer interfaces, the backbones are invariantly at proper distances. Since the sequences were modelled by means of spatial restraints on a single subunit (the crystal structure of the oxy-form of *Limulus* subunit II),⁶ the MODELLER procedure ignored the presence of any neighbouring subunit. Furthermore, the orientation of the side-chains is not necessarily optimal. Therefore, when necessary, an additional pair-wise fitting of subunits was performed, which eliminated the overlaps completely without moving the backbones (see below). Although further work might improve the present

Table 3. Amino acid residues involved in inter-hexamer interfaces

Interface	Residues in first subunit	Residues in second subunit
A. between the two 1×6mers of the 2×6mer		
II-II	Both subunits: ⁴⁰² HARVD ⁴⁰⁶ (399–403), H ⁴¹⁰ (407), F ⁴¹² (409), R ⁴¹⁴ (411), ⁴³⁶ YYHLDHEPFSY ⁴⁴⁶ (433–443), H ⁵⁰⁶ (503), K ⁶³⁰ (625), H ⁶³² (627)	
II-IV	² TLHD ⁷ (1–4), H ¹⁴ (11), F ⁷³ (70), ¹⁴⁰ EFDE ¹⁴³ (137–140), H ⁵²⁵ (522), H ⁵³² (529)	K ⁴⁰⁴ (398), H ⁴¹⁰ (404), F ⁴¹² (406), H ⁴⁴¹ (433), F ⁴⁴⁴ (436), R ⁴⁷⁶ (468), ⁶¹² RTPSQ ⁶¹⁶ (602–606), F ⁶³¹ (621), H ⁶³³ (623)
IV-VI	K ³⁸⁶ (380), E ³⁹³ (387), E ⁴⁵¹ (443), H ⁴⁵³ (445)	¹⁴⁰ HK ¹⁴¹ (139–140)
V-VI	Both subunits: ²⁶ KFALKAHRDPK ³⁶ (25–35), ⁷³ FEEFLDLCHQVRDF ⁸⁶ (072–85), Y ⁹² (91)	
B. between the two 2×6mers of the 4×6mer		
V-V	Both subunits: ² VL ³ (1–2)	
V-VI	⁴⁵⁴ TSK ⁴⁵⁶ (452–454), ⁵⁶⁸ HDQVGDH ⁵⁷⁴ (566–572)	²⁹⁰ DEN ²⁹² (288–290), ¹⁹⁰ EVIGKV ¹⁹⁵ (188–193)
VI-IIIB/IV/V	⁴⁵⁴ TSKTK ⁴⁵⁸ (452–456), H ⁴⁵³ (451), H ⁴⁹⁷ (495), H ⁵⁰⁰ (498), H ⁵⁶⁸ (566)	IIIB ²⁹² EGQE ²⁹⁵ (288–291), H ²⁸⁷ (283), H ²⁹¹ (287) IV ²⁹⁴ KE ²⁹⁵ (288–289), H ²⁸⁷ (281), H ²⁸⁹ (283), H ²⁹² (286) V ²⁹² NGS ²⁹⁴ (290–292), H ²⁸⁴ (282), H ²⁸⁷ (285), H ²⁹⁵ (293)
C. between the two 4×6mers of the 8×6mer		
IIIA-IIIA	Both subunits: ¹⁴⁰ DK ¹⁴¹ (136–137), H ¹³⁸ (134), H ⁴³⁰ (423)	
IIIA-IIIB	⁴⁵⁴ SGS ⁴⁵⁶ (447–449), K ⁵⁷⁴ (567)	E ³⁰¹ (297), D ⁴⁵⁴ (450)
II-IV	D ⁷² (69)	K ⁷¹ (67)
IV-IV	Both subunits: F ³⁹¹ (385), ⁴⁵⁵ DTVKH ⁴⁵⁹ (447–451), ⁴⁹² FHHGIHKGH ⁵⁰⁰ (484–492), ⁵⁶⁶ WE ⁵⁶⁷ (558–559), H ⁵⁷⁰ (562), E ⁵⁷⁴ (566)	

Superscript, relative residue numbers as in the text and in Figure 5. Parentheses, absolute residue numbers as in the crystal structure of *Limulus* II,^{5,6} and in the present molecular models of the different subunits.

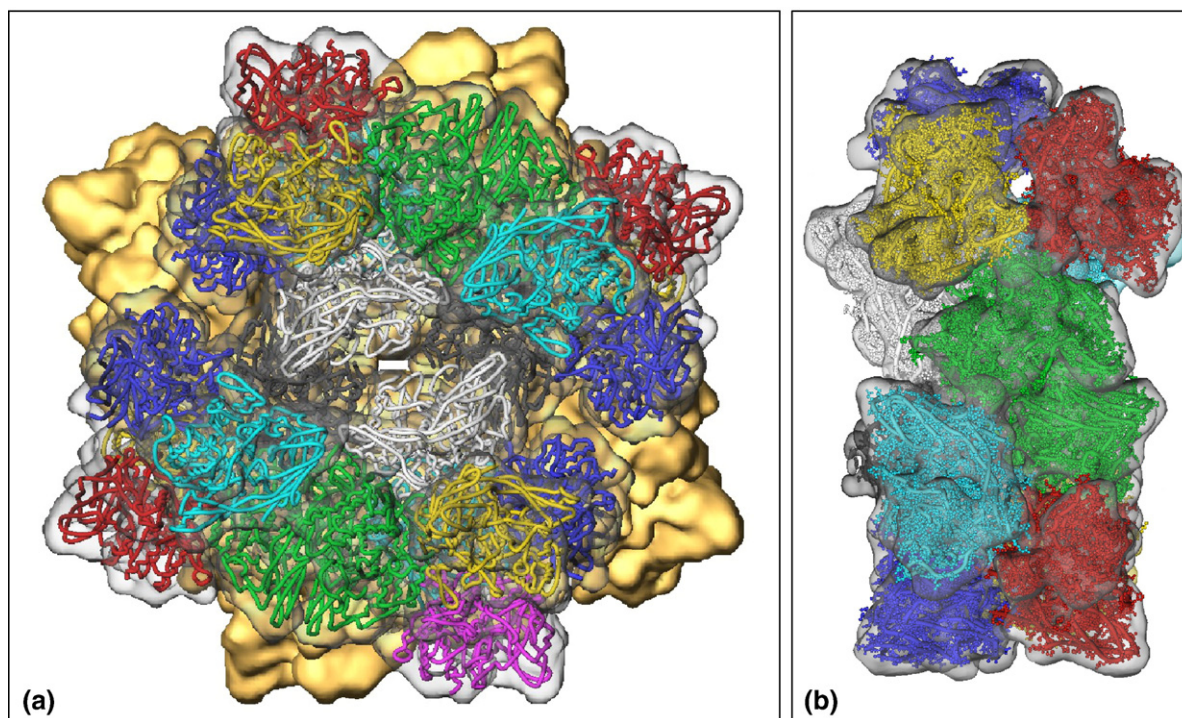


Figure 6. The 10 Å cryo-EM structure and molecular model of *Limulus* hemocyanin. (a) The 8×6mer (ring view orientation), with the lower 4×6mer represented as the cryo-EM structure (gold). The upper 4×6mer is shown as a molecular model (tube view representation of backbone), with the subunits colour-coded as in Figure 3, and the cryo-EM structure shell indicated (opaque). The molecular model of the whole 8×6mer includes the coordinates of ~30,000 amino acid residues, ~500,000 atoms. (b) The cryo-EM structure (opaque) and the molecular model of the extracted 2×6mer, to show the fitting of individual (colour-coded) subunits more clearly (backbone, tube view representation; side-chains, ball-and-stick representation, atomic volume set to 50%).

molecular model, it proved to be very suitable for assessing the molecular structure of the different inter-hexamer bridges.

Analysis of the inter-hexamer bridges

The crystal structure of arthropod hemocyanin subunits shows three different structural domains, here designated as #1, #2 and #3 (see Figure 5).^{4–6} Domain #2 contains the copper active site that is attached to four α -helices; this domain is usually not involved in any inter-hexamer contact, in contrast to the flanking domains #1 and #3. The N-terminal domain #1 is rich in α -helices, whereas the C-terminal domain #3 is dominated by a seven-stranded anti-parallel β -barrel and a long β -hairpin that reaches towards domain #1. As already mentioned, the molecular fitting revealed that in the molecular model of the 8×6mer, the subunits are not exactly arranged as in the isolated spiny lobster 1×6mer, but slightly deformed, notably those that are involved in inter-hexamer contacts. From the observation that *Limulus* 8×6mers can be dissociated into 4×6mers, 2×6mers and subunits by changing the ionic conditions, hydrostatic bonds should be primarily expected to establish the higher-order quaternary structure.⁴⁰ Details about the domains and amino acid residues involved in the inter-hexamer bridges to be discussed now are summarized in Table 3, the positions of the bridges are

shown in Figure 7, and the molecular interfaces are illustrated by Figures 8 ×10. The α -helices and β -strands as predicted from the crystal structure of *Limulus* subunit II are indicated in the present sequence (see Figure 5). The residue numbers given below conform to the numbering in this alignment, to allow the reader their clear identification. In addition to this relative numbering, the absolute residue numbers as obtained from molecular modelling are given in Table 3.

Bridges between the two 1×6mers of the 2×6mer

The 10 Å cryo-EM structure shows four different types of interface that yield six bridges (Figure 7(a)): a II–II interface with two sub-regions; a V–VI interface; two equivalent II–IV interfaces with two sub-regions; and a IV–V interface (on the flop face of the 4×6mer) with the equivalent IV–VI interface (on the flip face). Bridges between II–II, II–IV, and V–VI have been described,³⁸ whereas the IV–V (respectively IV–VI) bridge is new.

In the molecular model, the prominent II–II bridge is formed by complementary association of domain #3. In particular, both copies of the β -3A→ β -3B loop (⁴⁰²HARVD⁴⁰⁶) and the β -3C→ β -3D loop (⁴⁴⁰DHEPFSY⁴⁴⁶) are assembled into a rather dense structure to which other amino acid residues also contribute. This is in contrast to the kind of association predicted in the earlier studies.^{35,38}

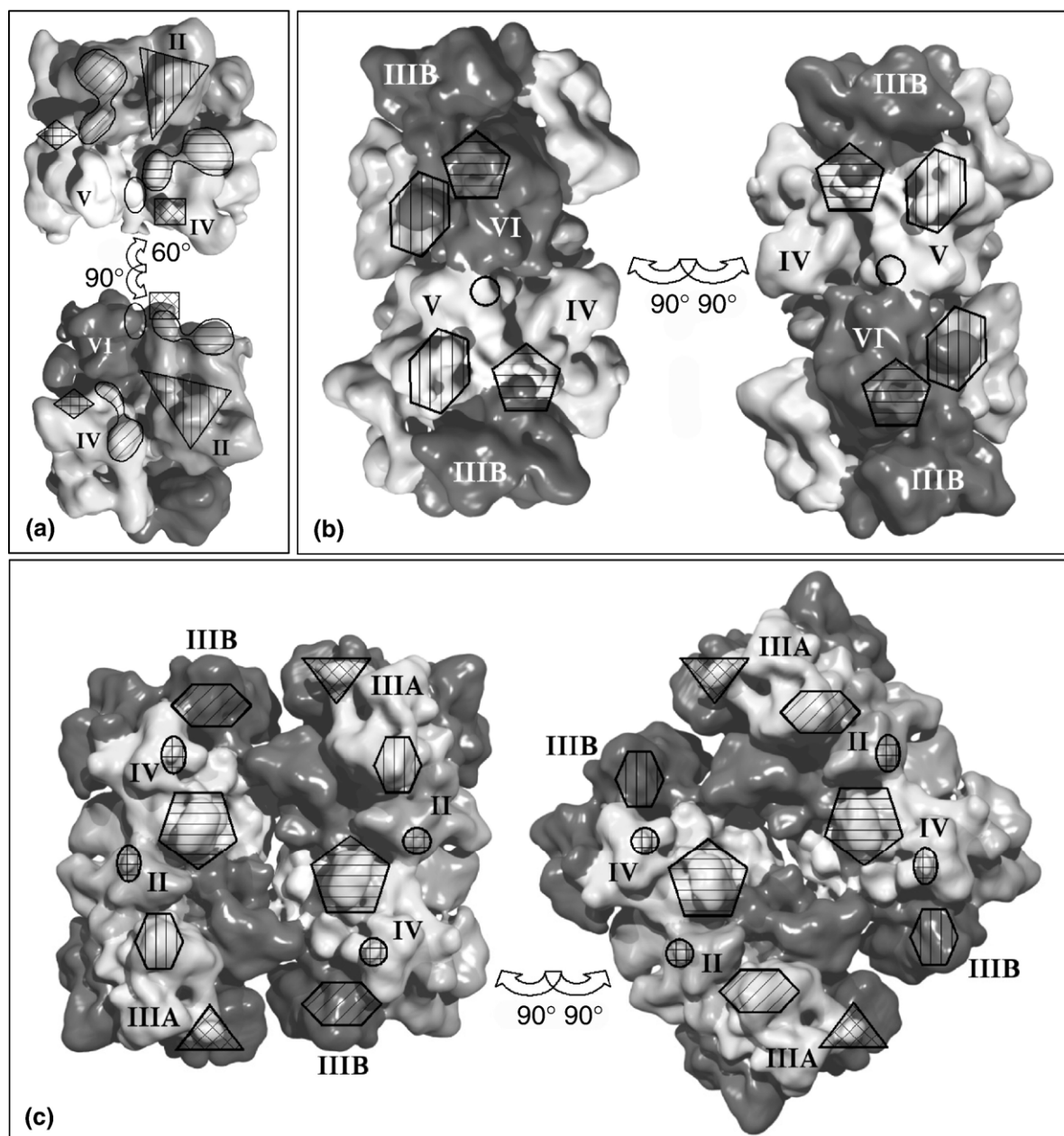


Figure 7. Topography of the inter-hexamer bridges. The respective hierarchy levels (2×6mer, 4×6mer, 8×8mer) are cut through their inter-hexamer bridges, and the cut surfaces exposed to the reader. Areas forming a joint interface (bridge) are marked by identical symbols. There exist eleven different types of interface that form a total of 46 inter-hexamer bridges within the 8×6mer. (a) Interfaces connecting the 1×6mers within the basic 2×6mer. Note that there are six bridges but only four types of interface, symbolized by ellipse (V–VI bridge), triangle (II–II bridge), rhombus/square (IV–V and IV–VI bridge that are structurally equivalent), and double field (II–IV bridge). (b) Interfaces connecting the 2×6mers within the 4×6mer. Note that there are five bridges but only three types of interface, symbolized by circle (V–V bridge), pentagon (VI–III B/IV/V bridge), and hexagon (V–VI bridge). (c) Interfaces connecting the 4×6mers within the final 8×6mer. Note that there are twelve bridges but only four types of interface, symbolized by circle/ellipse (II–IV bridge), triangle (III A–III A bridge), pentagon (IV–IV bridge), and hexagon (III A–III B bridge). Comparison to Figure 4(b) and (b') shows that the 4×6mers are assembled at their flip faces.

Initially, we thought that there might be some general overlapping at this interface, but we did indeed discover that the two subunits fit perfectly (apart from residues R404 and H506/D406, see below), and we revealed an intriguing contact apparatus (Figure 8(a) and (a')). The upper part is formed by two polypeptide backbones that run antiparallel and thus form a gap of 4–5 Å between

eight residues (A403, V405, E442 and P443). This motif might connect the two subunits *via* direct backbone interaction. There is an interesting association of four histidine residues (H402, H506), two serine residues (S445) and two aspartic acid residues (D406) arranged in a ring. (Initially, this association yielded a slight overlap of H506 and D406, which could be corrected by pair-wise remodelling.) This

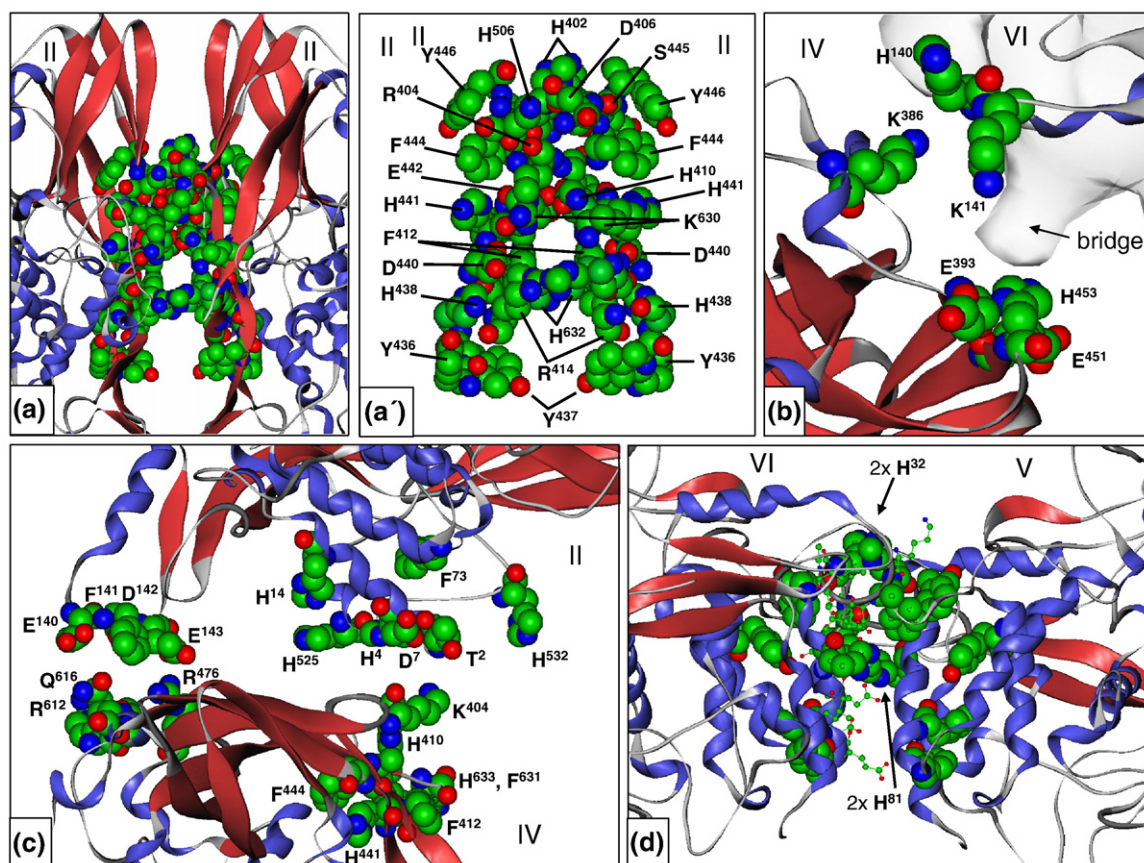


Figure 8. Molecular structure of the inter-1×6mer bridges in the 2×6mer. (a) and (a') Views of the II–II interface; for a detailed description, see the text. (b) The IV–VI interface; note the position of the bridge (arrow) in the cryo-EM structure (grey), indicating that the $^{140}\text{HK}^{141}$ turn might be modelled incorrectly. (c) The II–IV interface. Note the histidine/phenylalanine clusters that are associated with the contact zone shown on the right. (d) The V–VI interface; some residues are displayed with 0.25 atomic volume. The structure of this interface is ambiguous, because the authentic sequence of subunit V is still unknown.

ring is associated with four aromatic residues (F444 and Y446) that flank S445 in the sequence. The lower part of the II–II interface is composed of three aromatic residues ($^{436}\text{YYH}^{438}$) that form a tripartite screen around the peptide bond of R414 (see Figure 8(a')). Even more striking is the central part of the II–II interface. It is a chamber about 10 Å in diameter formed by six histidine residues (H410, H441, H632), two phenylalanines (F412), and four acidic residues (D440, E442). Within this chamber, the nitrogen atoms of two basic residues (R414) are brought together. Two additional arginine residues (R404) and two lysine residues (K630) flank the chamber. (Initially, the long residue R404 had not been modelled correctly, and overlapped with other atoms; this required remodelling). The chamber has two wide openings, and it is reasonable to presume that it permits the binding of an allosteric ligand, and that the acidic and basic residues form salt-bridges. Indeed, its components are also conserved in the orthologous subunit a of *Eurypelma hemocyanin*.²⁹ Allosteric interaction within the 8×6mer has somehow to be transferred between the hexamers. As deduced from low-resolution SAXS analyses, within the 2×6mer the rotation angle between the two hexamers is increased significantly upon deoxyge-

nation³⁶ (see Table 1). The II–II interface right at the centre of the 2×6mer is a very promising candidate for such an allosterically controlled rotation apparatus.

At the applied mass-correlated threshold there is a small inter-hexamer bridge between subunits IV and VI, and, due to the D2 point-group symmetry, there is an equivalent bridge between subunits IV and V. At this interface, only a few residues come together (distance ~6 Å); namely, K386 in α -helix 3.1 of subunit IV and $^{140}\text{HK}^{141}$ in the large α -1.7→ β -1B loop of subunit VI (Figure 8(b)). This association of three basic residues would require a bridging anion. However, we think that the positive charges prohibit bonding at this site. This is further emphasized by the fact that in the 10 Å cryo-EM structure, $^{140}\text{HK}^{141}$ is not exactly localized within the small bridge, but protrudes sideward (see Figure 8(b)). We therefore think that this loop is modelled incorrectly (although pair-wise remodelling of the two subunits did not change the situation.) Tilting this loop towards the bridge would bring $^{140}\text{HK}^{141}$ close enough to two glutamic acid residues (E393 and E451) exposed at the opposite side of the bridge. This site would then contain two closely associated histidine residues (H140 and H453), and it should be mentioned that

the histidine-rich C terminus of subunit IV is also in the neighbourhood. Whether this is of any functional significance remains to be investigated.

The II-IV interface is localized between domain #1 of subunit II and domain #3 of subunit IV, and is subdivided into two contact points: In the first, the N-terminal end of subunit II (²TLHD⁷) is connected to the β-3A→β-3B loop of subunit IV, indicating the presence of hydrostatic bonds between a lysine (K404) of subunit IV and a threonine/glutamic acid of subunit II (Figure 8(c)). Interestingly, this site is surrounded by various histidine and phenylalanine residues and therefore might contribute to allosteric interaction between hexamers. At the second contact point, the acidic α-1.7→β-1B loop of subunit II (¹⁴⁰EFDE¹⁴³) binds electrostatically to the basic-to-polar C-terminal α-helix 3.6 (⁶¹²RTPSQ⁶¹⁶) of subunit IV; the apolar phenylalanine F141 in subunit II probably shields the site from water molecules that could weaken the electrostatic bonding. Moreover, there is an opportunity for a strong salt-bridge between the second glutamic acid (E143) in subunit II and an arginine (R476) in the β-3E→α-3.2 loop of subunit IV (see Figure 8(c)). Some of these secondary structures have been predicted to be involved in this bridge.^{35,38}

On the basis of the 40 Å structure of *Limulus hemocyanin*, it has been proposed that the V-VI bridge is constructed from five different secondary structural elements.³⁸ From the present 10 Å structure, we can reduce this to α-helix 1.5. The two copies of this helix run parallel with each other and have a backbone distance of ~7 Å in the lower part and ~12 Å in the upper part (Figure 8(d)). From their orientation within this helix, the following residues potentially interact at the interface: ⁷³FEFLDLCHQVRDF⁸⁶. Since the sequence of subunit V is unknown, this interface cannot be described with certainty. With the sequence of subunit VI applied to both subunits, a few overlappings of side-chains are observed. The second element of interaction between subunit V and VI has been unpredicted, namely the sequence ²⁶KFALKAHRDPK³⁶ of the large loop following helix 1.1 and leading to the short helix 1.3. (It should be mentioned that helix 1.2 detected in *Panulirus hemocyanin* is missing from chelicerate hemocyanin.) The two equivalent loops are arranged in an antiparallel manner (see Figure 8(d)). Comparison of the loop sequence with the primary structures of the *Eurypelma hemocyanin* subunits²⁹ revealed that this motif is strictly conserved in both subunit b and subunit c, whereas the other subunit types are highly variable in this region. In the centre of this interface, we discovered a central histidine pair (H81; see Figure 8(d)) that form the floor of a cavity with a vertical width of ~10 Å. The roof of the cavity is primarily another histidine pair (H32). In the wall of the cavity, four phenylalanine residues (F27, F86) and two tyrosine residues (Y92, in the neighbored α-helix 1.6) are incorporated; four additional phenylalanine residues (F73, F76) beneath the cavity surround four glutamic acid

residues (⁷⁴EE⁷⁵). We think that, like the II-II bridge, the V-VI interface might be involved in transferring allosteric interaction between the two hexamers. Since many residues forming this interface are conserved in *Eurypelma* subunits b and c (except H32), there is a good chance that *Limulus* subunit V possesses them, and modelling with the sequence of subunit VI might be justified to describe this bridge. Nevertheless, further analysis of this interface requires the authentic sequence of subunit V.

Bridges between the two 2×6mers of the 4×6mer

As shown in Figure 7(b), three types of interface between the two 2×6meric halves of a 4×6mer can be identified in the 10 Å cryo-EM structure, yielding a total of five bridges: two equivalent VI-IIIb/IV/V interfaces at the flip face, two equivalent V-VI interfaces at the flop face, and a small V-V interface at the flop face. It should be kept in mind that the designations V and VI are interchangeable: It remains unknown as to which is which, and consequently, we do not know which of these two positions corresponds to the amino acid sequence of subunit VI.

On the flop face of the 4×6mer, a tiny bridge crosses the narrow cleft between the two copies of subunit V. As shown in Figure 9(a), this bridge is due to interaction of the two N termini (²VL³); these residues are identical in subunits V and VI, as known from N-terminal sequencing,²⁰ but the bridge cannot be formed between subunits VI because of their larger distance (see Figure 7(c)). The bridge is not visible in the cryo-EM density map, at the mass-correlated threshold, but it is detectable if the threshold is decreased slightly.

The V-VI bridge is subdivided into two adjacent contact points (Figure 9(b)). In one, the β-2D→β-2E loop of subunit VI (²⁹⁰DEN²⁹²) joins the β-3D→β-3E loop of subunit V (⁴⁵⁴TSK⁴⁵⁶), which indicates hydrostatic interaction; however, the sequence of subunit V is unknown and the sequence of VI has been used instead. At the other contact point, the situation is not well defined, because the large loop following α-helix 3.5 in subunit V has apparently been modelled incorrectly and protrudes from the cryo-EM structure. To form the second contact point, this loop seems to interact with its region ⁵⁶⁸HDQVGDH⁵⁷⁴ to the region ¹⁹⁰EVIGKV¹⁹⁵ of the α-2.1→α-2.2 loop of subunit VI. An interaction between D573 and K194 is indicated, but in the case of subunit V it is not the authentic primary structure. Thus, the details of this second contact remain obscure, and the whole interface requires further research. It should be noted, however, that the sequence of subunit VI provides a number of histidine residues in this area.

The analogous β-3D→β-3E loop in subunit VI does not point directly towards the β-2D→β-2E loop of subunit V, but is closer to the central hole of the opposing hexamer. There, it also joins the two other subunits of the flip face of this hexamer; namely, IV and IIIb (Figure 9(c)). This VI-IIIb/IV/V

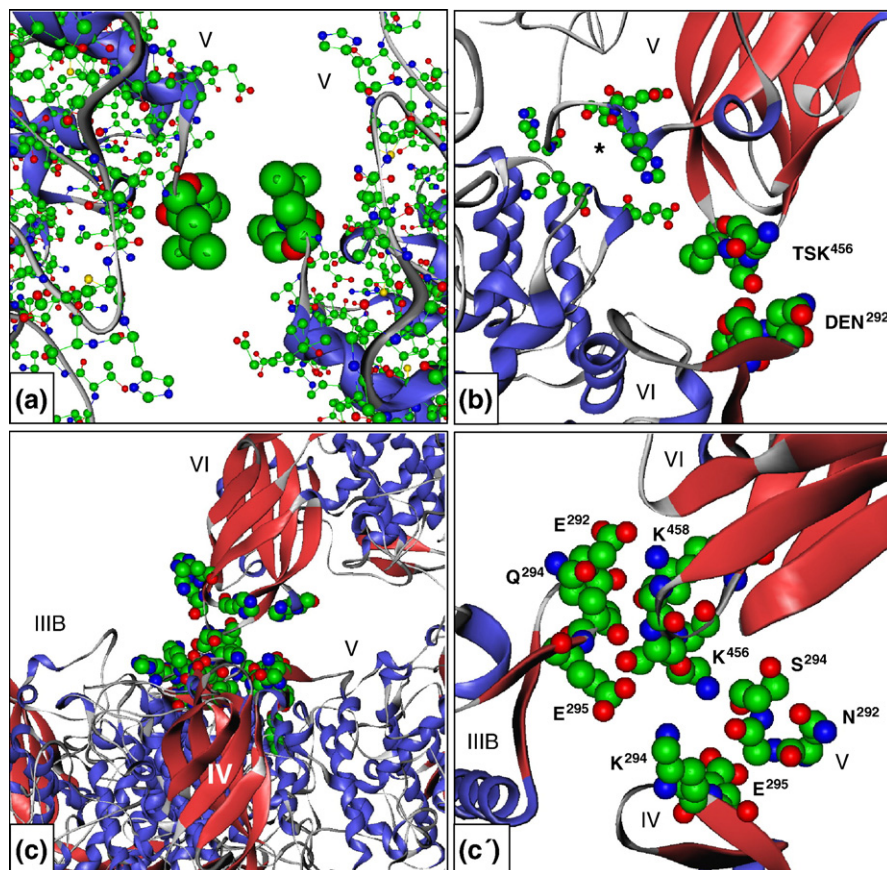


Figure 9. Molecular structure of the inter-2×6mer bridges in the 4×6mer. (a) The V–V interface, formed by the N-terminal residues valine and leucine; the other residues are shown in 0.25 atomic volume. (b) The V–VI interface. It remains unclear which residues form the second contact (asterisk); the candidate residues in this area are shown with 0.25 atomic volume. (c) (c') The VI–III A/IV/V interface. In (c), the adjacent histidine residues are highlighted in addition to the candidate residues for chemical bonding; the latter are shown exclusively in (c').

interface could not be predicted from the earlier 40 Å resolution structure,³⁸ but is highly significant with respect to our search for centres of allosteric transmission: There is evidence from X-ray crystallography that within the 1×6mer, the two subunit trimers behave as rigid bodies that can rotate 3.2° with respect to each other around their 3-fold axis upon oxygenation.^{5,6} Such a rotation would dislocate the VI–III B/IV/V bridge, and by domain #3 of subunit VI acting as a lever, a power transmission to the opposing 2×6mer is possible. The β-3D→β-3E loop of subunit VI (⁴⁵⁴TSKTK⁴⁵⁸) joins β-strand 2E of subunit IV at ²⁹⁴KE²⁹⁵, and electrostatic bonding is likely to occur between them (Figure 9(c')). To this site, β-strand 2E of subunit V contributes ²⁹²NGS²⁹⁴ (although this might not hold true in the authentic sequence of V), and subunit III B (with the orthologous sequence of *Eurypelma* subunit f applied) delivers residues ²⁹²EGQE²⁹⁵ in β-strand 2E (see Figure 9(c')). Most interestingly, this central cluster of charged residues is surrounded by 12 histidine residues (see Figure 9(c)) brought together from all four subunits (III B, H287, H291; IV, H287, H289, H292; V, H284, H287, H295; and VI, H453, H497, H500, H568). Therefore, the VI–III B/IV/V interface is indeed a promising candidate for transferring

allosteric interaction from one 2×6mer to the other. It differs from the V–VI bridge in two aspects: the joining of four different subunits in a single small site, and the lack of the second anchor point (see Figure 9(b)).

Bridges between the two 4×6mers of the 8×6mer

In the 10 Å cryo-EM structure, four different types of interface can be identified that together provide 12 bridges between the two 4×6mers (Figure 7(c)). Most prominent are two central, structurally equivalent IV–IV bridges. According to reassembly experiments, subunit IV is stringently required for 8×6mer formation.^{27,40,41} The other contacts are arranged in two peripheral arcs around the central IV–IV bridges (see Figure 7(c)). We identified four equivalent II–IV bridges, four equivalent III A–III B bridges, and two equivalent III A–III A interfaces. It is interesting to note that in reassembly experiments, in addition to subunit IV, subunit III A proved to be indispensable for higher-order assembly beyond the 4×6mer.²⁰ Except for the III A–III A bridge, the contact regions are invariantly located on the edges of the V-shaped cleft between the two 2×6mers (see Figure 4(c)). A IV–IV bridge as well as a III A–III B bridge

have been described,³⁸ the other two interface types (II–IV and IIIA–IIIa) are new.

The IIIA–IIIa bridge is easily detected in the cross-view representation of the 10 Å cryo-EM structure (see Figures 3(c') and 6(c)) and is formed between domains #1 and #3. The fitted ternary structures revealed a most interesting interface (Figure 10(a)). It is formed by two copies of ¹⁴⁰DK¹⁴¹ in the α -1.7→ β -1B loop, which suggests the presence of two strong salt-bridges between the two subunits. The distance between the two potential binding atoms in the molecular model is 4.5 Å. This arrangement is closely associated with four histidine residues (H138 in the same loop and H430 in the β -3B→ β -3C loop); their aromatic rings occupy the corners of a tetrahedron with edge length of 8 Å. Viewed from the top, the four histidine residues expose a wide opening, probably for a ligand (Figure 10(a')). Due to its peripheral position and oblique orientation between the two 4×6mers (see Figures 3(b) and 6(c)), chemical changes within the two IIIA–IIIa bridges (that are localized at opposite surfaces of the 8×6mer) might result in a slight rotation of the two 4×6mers with respect to each other around their staggering axis. This could transmit forces over long distances and thereby mediate allosteric interaction between the two 4×6mers.

The intricate molecular structure of the IIIA–IIIa interface is very promising with respect to this role.

The small IIIA–IIIb bridges are not visible in the cryo-EM density map at the mass-correlated threshold, but they appear if the threshold is decreased slightly. In the case of IIIb, the orthologous sequence of *Eurypelma* hemocyanin (subunit f) was applied; however, since *Eurypelma* hemocyanin is a native 4×6mer, it could be expected that regions involved in inter-4×6mer bridges differ in the two sequences. Other workers have described a IIIA–IIIb bridge, but their predicted sites differ completely from those found in the present study.³⁸ We detected potential linkages between both domains #3, and between domain #3 of subunit IIIa and domain #2 of subunit IIIb (Figure 10(b)). To the #3–#3 contact, IIIa contributes lysine K574 in the loop following helix α -3.5; to the #3–#2 contact it delivers the sequence ⁴⁵⁴SGS⁴⁵⁶ in the β -3D→ β -3E loop. This indicates the presence of hydrostatic bonds in both cases. Indeed, with the orthologous *Eurypelma* type f sequence applied for IIIb, at a proper distance acidic residues (D454 in the β -3D→ β -3E loop, E301 in the β -2.E→ α -2.4 loop) are available for bonding (see Figure 10(b)). However, the correct description of this bridge requires the authentic primary structure of subunit IIIb.

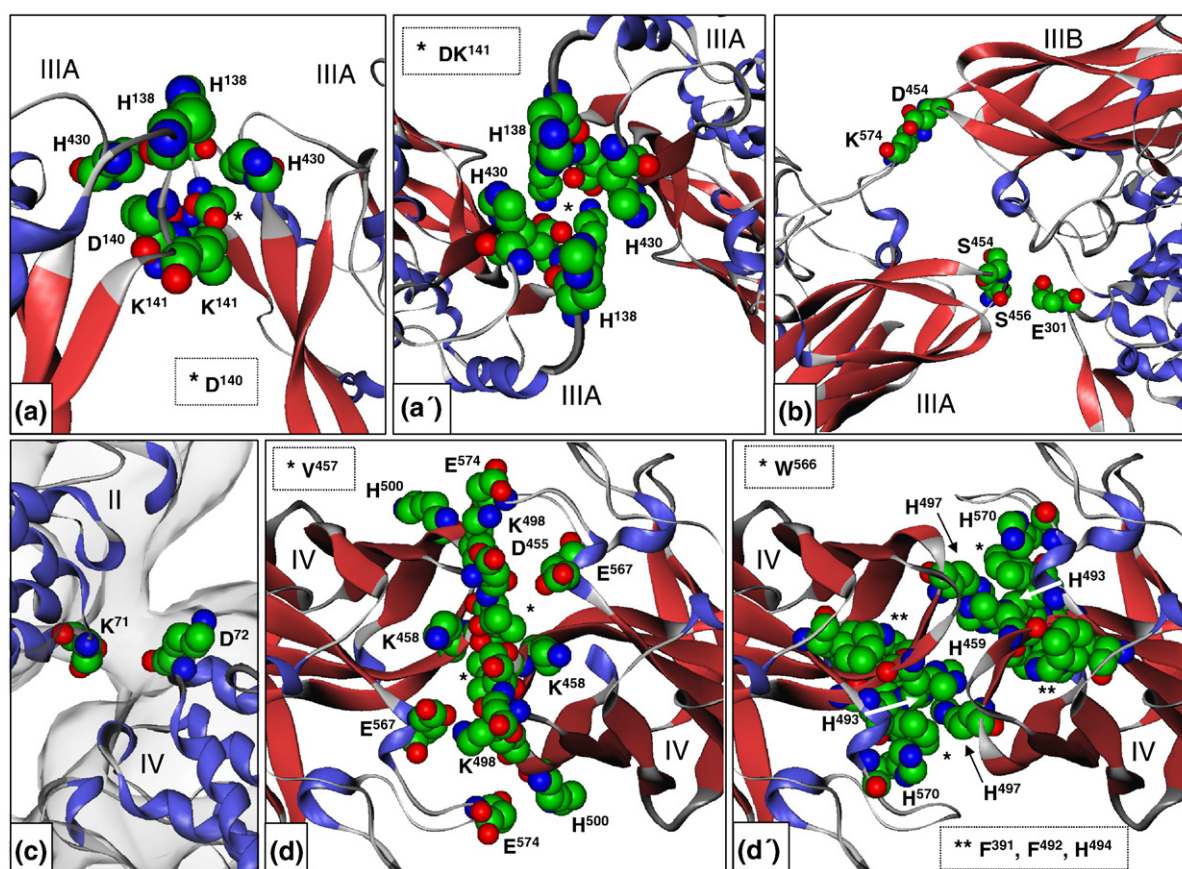


Figure 10. Molecular structure of the inter-4×6mer bridges in the 8×6mer. (a) and (a') The IIIA–IIIa interface; note the close association of four histidine residues with the charged residues. (b) The IIIA–IIIb interface. (c) The II–IV interface. (d) and (d') The IV–IV interface. (d) The candidate residues for chemical bonding. (d') The two compact associations of a tryptophan residue (W566) with four histidine residues are shown, together with additional phenylalanine and histidine residues. Note that H497 is delivered to these “wheelhouses” by the opposite subunit.

The II–IV bridge is localized, in both subunits, at exactly the same position in the α -1.4→ α -1.5 loop. Ionic bonding is possible between residue D72 of subunit II and residue K71 of subunit IV (Figure 10(c)); all other possibilities can be excluded on the basis of the distances. As can be seen in Figure 10(c), the lysine residue points in the wrong direction, but this might be due to incorrect modelling. The backbone distance between the two amino acid residues is ~ 10 Å, which is easily bridged if the two residues were oriented towards each other.

In the prominent, somewhat oblique, IV–IV bridge, three regions of domain #3 are involved (see Table 3), which, in principle, were traced in the earlier 40 Å structure.³⁸ Now, they could be more firmly identified as ⁴⁵⁵DTVKH⁴⁵⁹ in the β -3D→ β -3E loop, ⁴⁹²FHHGIHKGH⁵⁰⁰ from β -strand 3G to β -strand 3H, probably phenylalanine F391, and several amino acid residues in α -helix 3.5 and the following loop (⁵⁶⁶WE⁵⁶⁷, H570, and E574). Although this loop is missing from the X-ray structure of *Limulus* II hemocyanin, we found very few overlaps of side-chains in this region. These overlaps could be eliminated by a joint remodelling of the two subunits (see above), which did not influence the backbone, but re-oriented several side-chains and resulted in a perfect fit at the interface. Despite the numerous amino acid residues involved in this site, a clear and fascinating picture emerges (Figure 10(d) and (d')). This interface contains the following elements: The relevant secondary structures from both subunits are arranged in an antiparallel manner, and their equivalent turns ⁴⁵⁵DTVKH⁴⁵⁹ join each other at 4 Å distance. This assembles the two hydrophobic valine residues (V457) that apparently help to bind the two turns together (see Figure 10(d)). This binding might be reinforced by hydrostatic interaction between the charged residues D455, T456 and K458 delivered from both subunits. More peripheral at either flank of the interface, bonding is likely to occur between K498 and E567, as well as between H500 and E574 (see Figure 10(d)). The clue to this interface, however, is two equivalent residue clusters that resemble minute “wheelhouses”; they are located at either side of the joined turns (see Figure 10(d')). The “wheel” is the central C-6 ring of a tryptophan (W566), and the “house” is four closely associated histidine residues (H459, H493, H497 and H570) that surround the tryptophan. An additional histidine (H494) and two phenylalanine residues (F391 and F492) are in the neighbourhood (at 8–10 Å from the tryptophan), but it is not clear whether they contribute to this site. It is probably more significant that one of the four central histidine residues (H497), with a ring-to-ring distance of only 2–3 Å to the tryptophan, comes from the opposite subunit. If the tryptophan was dislocated with respect to H497 by an allosteric effect, this could transmit forces between the opposite backbones to change their distance. This, in turn, would change the length of the IV–IV bridge and, due to its oblique orientation, this would change the staggering angle between the two 4×6mers. It appears that the two IV–IV bridges (together with the two IIIA–IIIA bridges

between the alternating hexamers; see Figure 7(c)) have the potential to transmit allosteric interaction between the 4×6mers.

Concluding remarks

In conclusion, 11 types of inter-hexamer interface have been identified in the present 10 Å structure; which, in the native 8×6mer sum up to 46 inter-hexamer bridges: there are 24 within the four 2×6mers, ten to establish the two 4×6mers, and 12 to assemble the two 4×6mers into an 8×6mer. From advanced molecular modelling and rigid-body fitting, each of these interfaces has been assigned to very few amino acid residues that now serve as candidates for the chemical bonds between the eight hexamers. In chelicerate hemocyanins, all hierarchical levels of the protein are involved to establish the oxygen-binding properties, and reveal a stepwise decrease of cooperativity from 4×6mers to 2×6mers to 1×6mers,^{36,42,43} consequently, allosteric interaction has to be somehow transferred *via* the inter-hexamer bridges. Several intriguing structures have now been unravelled as possible mediators of allosteric signals between the different levels of the nested hierarchy: the II–II interface, the II–IV interface and the V–VI interface between the 1×6mers, the VI–IIIB/IV/V interface between the 2×6mers, the IIIA–IIIA interface and the IV–IV interface between the 4×6mers. The present *Limulus* hemocyanin preparation has been studied under oxygen saturation conditions, in the presence of 25% oxygen, to produce vitrification of the protein molecules in their fully oxygenated state (under physiological conditions usually the R-state). Indeed, the retrieved parameters of the *Limulus* 4×6mer convincingly fit the SAXS model of the oxy-4×6mer of *Eurypelma*,³⁶ whereas the deoxy-4×6mer SAXS model is significantly different (see Table 1). We are optimistic that the same procedure, carried out under oxygen-free conditions (i.e. in 100% nitrogen), will produce the hemocyanin molecule in its fully deoxygenated state (usually the T-state). A 3D reconstruction and analysis at a comparable resolution should then show the different inter-hexamer bridges in the deoxygenated 8×6mer, which might assist the understanding of how, during oxygen binding, allosteric signals are structurally transferred between the different levels of the oligomeric hierarchy. Thus, the present 10 Å structure opens the door to a fundamental understanding of the function of this highly cooperative protein.

Materials and Methods

Animals

Several *L. polyphemus* were obtained from the Marine Biolab (Woods Hole, USA). They were kept in artificial seawater at 18 °C (12 h light /12 h dark cycle); and were fed on fish.

Hemocyanin purification

Hemolymph was withdrawn from living animals at the prosoma-opisthosoma joint by inserting the needle of a syringe into the dorsal sinus. The blue hemolymph was centrifuged for 30 min at 3300g. The cell-free supernatant was then centrifuged for 2 h at 130,000g. The hemocyanin pellets were resuspended in a low-salt buffer, (100 mM Tris-HCl (pH 7.8), 10 mM CaCl₂, 10 mM MgCl₂).

Preparation and cryo-electron microscopy

Rapid freezing/vitrification was performed as described.⁴⁴ A droplet of the purified protein at a concentration of 0.1–0.3 mg/ml was applied to a glow-discharged holey carbon support film. After removing excess fluid by blotting, the grid was frozen by plunging it in liquid ethane under a controlled oxygen-containing atmosphere in a plunging tube. A constant stream of gas from the top to the bottom of the tube provided a stable and controlled condition during plunging. For the oxygenated state of the hemocyanin, a gas stream of 25% (v/v) O₂/75% (v/v) N₂ was used, and the sample was equilibrated for 2 min (exchange rate of gas volume: 23 tube volumes/min). The hemocyanin cryo-transfer was performed using a Gatan model 626 single-tilt cryo-transfer system (Gatan, Munich, Germany). Electron micrographs were recorded under low-dose conditions at an instrumental magnification of 59,000×. The underfocus was set between 1.0 μm and 5.0 μm. The negatives (Kodak SO 163 film) were developed for 12 min in full-strength Kodak D19 developer.

Image processing

Drift- and astigmatism-free electron micrographs were scanned and digitized using a PRIMESCAN drum scanner (Heidelberger Druckmaschinen AG, Heidelberg, Germany). The micrographs were scanned with 1.8 Å and 1.0 Å step size corresponding to 10.6 μm and 5.9 μm, respectively, on the negative. Image processing was performed mainly with the IMAGIC-5 software package.⁴⁵ Images of single particles were selected semi-automatically with the module BOXER from the EMAN 1.7 software package, which also allowed the processing of focal pair micrographs. Estimation of the defocus and astigmatism parameters was performed with the program CTFIND3, and CTF correction with the module TRANSEFER from IMAGIC-5. CTF-corrected images were band-pass filtered and normalized.

The first data set (focal pairs) with a scanning step size of 1.8 Å comprised 8984 single particles (for both high and low defocus), the second data set with a scanning step of 1 Å comprised 3085 single particles. Analysis started with a “reference-free alignment” of the 8984 single particles with a high defocus. Images of the data set were translationally centred according to their rotationally averaged total sum, maintaining the original rotational orientation of every single image. The following multi-variate statistical analysis (MSA), hierarchical ascendant classification and image averaging identified similar images with comparable orientations and produced class averages with improved signal-to-noise ratio. These improved class averages were then used to start an unbiased multiple reference alignment (MRA).⁴⁵ After two alignment refinements, three projections that represented a top, a tilted and a side-view were selected and the Euler angles assigned. These three projections were used

as an “anchor-set” for the remaining data set and, after angular reconstitution, a preliminary 3D reconstruction was calculated. Reprojections of the first reconstruction were used for the next round of MRA and MSA.

With the first data set with the scanning step of 1.8 Å, 17 rounds of refinements were run. In the first refinement rounds, the number of hemocyanin particles was increased progressively by adding single particles from the micrographs with a low defocus. After ten refinement rounds, the single particles from the micrographs with a high defocus were eliminated, leaving only images with a low defocus in the data set. The second data set comprising only images with a low defocus was down-sampled to fit the scanning step size of 1.8 Å of the first data set. Then, both data sets were combined and another five refinement rounds with a total of 12,069 single particles were run. The whole data set was distributed between 800 class averages (with an average of ~15 particles/class). The 3D reconstructions were calculated using the exact filter back-projection method with imposed D2 symmetry. Refinement steps were performed iteratively with calculated 3D reconstructions. The final projection-matching step was performed with the modelled PDB file of the 8×6mer as reference. The resolution was assessed by FSC of two halves of the data set. The final reconstruction was filtered to a nominal 10 Å, thus eliminating structural details beneath this cut-off.

Molecular modelling and fitting

The models of the different sequences were built using the MODELLER 7v7 software and the 3D structure of the *L. polyphemus* subunit type II hemocyanin (RSCB PDB code 1NOL) as template. Since the sequences for the subunits type I, IIA, IIIB and V were not available, the orthologous sequences of *E. californicum* subunit type e (I, IIA) and type f (IIIB) were used.^{20,22} Because subunit types V and VI are immunogenically very similar, subunit type VI was used instead of subunit type V. For each sequence, 20 different models were calculated. The alignments of the sequences for modelling were calculated with the CLUSTALX 1.81 software. The cryo-EM densities of the 24 subunits of the 4×6mer (one-half of the whole molecule) were isolated with the ResolveRT software (TGS Europe, Düsseldorf, Germany). A generous and roughly subunit-shaped mask was placed around every subunit and then multiplied with the whole density map, generating cryo-EM density maps of the isolated subunits. The latter were exported into the CCP4 file format for the molecular fitting procedure. All of the 20 models for each sequence were fit preliminarily into their respective cryo-EM subunit density with the MOLREP 9.2 software. The model with the highest score was then chosen. We considered this an objective approach of selecting a model from a number of possibilities.

The eight chosen molecular models (one for each subunit type) were then fit independently in the cryo-EM density map of the 8×6mer that was low-pass filtered to a nominal 8 Å but left unmasked. Fitting was done with a newly developed rigid-body fitting tool, creating eight homo-8×6mers. Given the very large dataset (170³ voxels), we have implemented a novel optimized docking program termed eliquos (J.H. & W.W., unpublished) that processes large datasets efficiently while maintaining compatibility with the exhaustive search methodology of the colores tool of the Situs fitting package.⁴⁶ The improved efficiency is achieved by an extensive use of computational geometry algorithms (J.H. & W.W., unpublished). Laplacian filtering of both the cryo-EM density

map and the molecular models was employed.⁴⁶ For each subunit, a six-dimensional grid-based exhaustive search was performed using an angular step size of 20° and a grid spacing of 1.8 Å. A distance-dependent pruning algorithm (J.H. & W.W, unpublished) then reduced the number of solution candidates to 48. The resulting subunit positions were optimized individually at sub-voxel accuracy using an off-lattice Powell optimization algorithm.⁴⁶ The final subunit fitting was assembled with the CHIMERA version 1 Build 2199 software by choosing the molecular modelled subunit types according to their respective topological positions within the 8×6mer.

Cloning and sequencing of hemocyanin cDNAs

Hematopoiesis was induced by bleeding *L. polyphemus* individuals about one week before RNA preparation. Animals were immobilized for several hours on ice and killed by cutting the ventral nerve cord. The inner organs were immediately removed and shock-frozen in liquid nitrogen. The tissue was ground to a fine powder with continuous addition of liquid nitrogen. Total RNA was extracted using the guanidine thiocyanate method.⁴⁷ Poly (A)⁺ RNA was purified by means of the PolyAtract kit (PROMEGA). A directionally cloned cDNA expression library was established using the Lambda ZAP-cDNA synthesis kit from STRATAGENE. The library was amplified once and screened with various specific anti-*Limulus*-hemocyanin antibodies. Positive phage clones were converted to pBK-CMV plasmid vectors with the material provided by STRATAGENE according to the manufacturer's instructions and sequenced on both strands by the commercial GENTerprise (Mainz, Germany) sequencing service. Complete hemocyanin cDNA sequences were obtained by the primer walking method using specific oligonucleotides.

Sequence analyses and molecular phylogenetic studies

The cDNA sequences were assembled by hand with the aid of GeneDoc 2.6.† The web-based tools provided by the ExpASY Molecular Biology Server of the Swiss Institute of Bioinformatics‡ were used for analyses of DNA and amino acid sequences. The amino acid sequences of the *L. polyphemus* hemocyanin subunits were added by hand to published alignments of chelicerate hemocyanin sequences.^{30,31} The chelicerate hemocyanin sequences were: *E. californicum* hemocyanin subunits a (accession number X16893), b (AJ290429), c (AJ277489), d (AJ290430), e (X16894), f (AJ277491) and g (AJ277492), *Nephila inaurata madagascariensis* hemocyanin subunits a (AJ547807), b (AJ547808), d (AJ547809), e (AJ547810), f (AJ547811) and g (AJ547812), *Tachypleus tridentatus* hemocyanin subunit alpha,¹¹ *Androctonus australis* hemocyanin subunit 6 (P80476), *Cupiennius salei* hemocyanin subunits 1 (AJ307903), 2 (AJ307904), 3 (AJ307905), 4 (AJ307906), 5 (AJ307907) and 6 (AJ307909). Four crustacean hemocyanin sequences, *P. interruptus* hemocyanin subunits a (P04254) and c (S21221), *Homarus americanus* hemocyanin A (AJ272095) and *Pacifastacus leniusculus* hemocyanin (AF522504), were included in the alignment and used as outgroups for tree rooting. The final alignment is available from the authors upon request.

Bayesian phylogenetic analyses were performed with MrBayes 3.1.⁴⁸ The WAG model of amino acid substitution⁴⁹ with gamma distribution of rates was applied. Metropolis-coupled Markov chain Monte Carlo sampling was performed with four chains that were run for 100,000 generations. Prior probabilities for all trees were equal, starting trees were random, trees were sampled every tenth generation. Posterior probability densities were estimated on the final 5000 trees (burn-in = 5000).

Database accession numbers

The cryo-EM density map of the *L. polyphemus* 8×6mer has been deposited in the EMD database (EMBL-EBI) under the accession number EMD-1304.

The *L. polyphemus* cDNA sequences have been deposited in the EMBL/GeneBank databases under the accession numbers AM260213 (subunit II), AM260214 (subunit IIIA), AM260215 (subunit IV), and AM260216 (subunit VI).

Acknowledgements

We thank Professor Dr J. Robin Harris for critical reading of the manuscript and language corrections. J.M. is indebted to Professor Dr Heinz Decker and Professor Dr Walter Stöcker for fruitful discussions. We thank Thorsten Schweikhardt for valuable information concerning parameters of the *Eurypelma* 4×6mer derived from SAXS analyses. This work was supported by grants to J.M. from the DFG (Ma843, GK 1043), the Stiftung Rheinland-Pfalz für Innovation (15202386261548), the Landesexzellenzcluster "Immunointervention" of Rheinland-Pfalz and the Elektronenmikroskopiezentrum Mainz (EMZM); a grant to T.B. from the DFG (Bu956/9); grants to W.W. from NIH (1R01GM62968), the Human Frontier Science Program (RGP0026/2003), and the Alfred P. Sloan Foundation (BR-4297).

References

1. Markl, J. & Decker, H. (1992). Molecular structure of the arthropod hemocyanins. *Advan. Comp. Environ. Physiol.* **13**, 325–376.
2. van Holde, K. E. & Miller, K. I. (1995). Hemocyanins. *Advan. Protein Chem.* **47**, 1–81.
3. Bergmann, S., Lieb, B., Ruth, P. & Markl, J. (2006). The hemocyanin from a living fossil, the cephalopod *Nautilus pompilius*: protein structure, gene organization, and evolution. *J. Mol. Evol.* **62**, 362–374.
4. Volbeda, A. & Hol, W. G. J. (1989). Crystal structure of hexameric hemocyanin from *Panulirus interruptus* refined at 3.2 Å resolution. *J. Mol. Biol.* **209**, 249–279.
5. Hazes, B., Magnus, K. A., Bonaventura, C., Bonaventura, J., Dauter, Z., Kalk, K. H. & Hol, W. G. (1993). Crystal structure of deoxygenated *Limulus polyphemus* subunit II hemocyanin at 2.18 Å resolution: clues for a mechanism for allosteric regulation. *Protein Sci.* **2**, 597–619.
6. Magnus, K. A., Hazes, B., Ton-That, H., Bonaventura, C., Bonaventura, J. & Hol, W. G. J. (1994). Crystallographic analysis of oxygenated and deoxygenated

† <http://www.psc.edu/biomed/genedoc/>

‡ <http://www.expasy.org>

- states of arthropod hemocyanin shows unusual differences. *Proteins: Struct. Funct. Genet.* **19**, 302–309.
7. Magnus, K. A., Lattman, E. E., Volbeda, A. & Hol, W. G. J. (1991). Hexamers of subunit II from *Limulus* hemocyanin (a 48-mer) have the same quaternary structure as whole *Panulirus* hemocyanin molecules. *Proteins: Struct. Funct. Genet.* **9**, 240–247.
 8. Jaenicke, E. & Decker, H. (2004). Functional changes in the family of type 3 copper proteins in evolution. *Chem. Biol. Chem.* **5**, 163–176.
 9. Burmester, T. (2001). Molecular evolution of the arthropod hemocyanin superfamily. *Mol. Biol. Evol.* **18**, 184–195.
 10. Burmester, T. (2002). Origin and evolution of arthropod hemocyanins and related proteins. *J. Comp. Physiol. B.* **172**, 95–117.
 11. Linzen, B., Soeter, N. M., Riggs, A. F., Schneider, H. J., Schartau, W., Moore, M. D. *et al.* (1985). The structure of arthropod hemocyanins. *Science*, **229**, 519–524.
 12. Markl, J., Burmester, T., Decker, H., Savel-Niemann, A., Harris, J. R., Süling, M. *et al.* (1992). Quaternary and subunit structure of *Calliphora* arylphorin as deduced from electron microscopy, electrophoresis, and sequence similarities with arthropod hemocyanin. *J. Comp. Physiol.* **162**, 665–680.
 13. Markl, J. (1980). Hemocyanin in spiders, XI. The quaternary structure of *Cupiennius* hemocyanin. *J. Comp. Physiol.* **140**, 199–207.
 14. Markl, J. (1986). Evolution and function of structurally diverse subunits in the respiratory protein hemocyanin from arthropods. *Biol. Bull. (Woods Hole)*, **171**, 90–115.
 15. Boisset, N., Taveau, J.-C. & Lamy, J.-N. (1990). An approach to the architecture of *Scutigera coleoptrata* hemocyanin by electron microscopy and image processing. *Biol. Cell*, **68**, 73–84.
 16. Brouwer, M., Bonaventura, C. & Bonaventura, J. (1977). Oxygen binding of *Limulus polyphemus* hemocyanin: allosteric modulation of chloride ions. *Biochemistry*, **16**, 3897–3902.
 17. Dolashka-Angelova, P., Dolashki, A., Stevanovic, S., Hristova, R., Atanasov, B., Nikolov, P. & Voelter, W. (2005). Structure and stability of arthropod hemocyanin *Limulus polyphemus*. *Spectrochim. Acta*, **61**, 1207–1217.
 18. Bijlholt, M. M. C., van Heel, M. G. & van Bruggen, E. F. J. (1982). Comparison of 4x6-meric hemocyanins from three different arthropods using computer alignment and correspondence analysis. *J. Mol. Biol.* **161**, 139–153.
 19. Brenowitz, M., Bonaventura, J., Bonaventura, C. & Gianazza, E. (1981). Subunit composition of a high molecular weight oligomer: *Limulus polyphemus* hemocyanin. *Arch. Biochem. Biophys.* **210**, 748–761.
 20. Lamy, J., Lamy, J., Sizaret, P.-Y., Billiald, P., Jolles, P., Feldmann, R. J. & Bonaventura, J. (1983). Quaternary structure of *Limulus polyphemus* hemocyanin. *Biochemistry*, **22**, 5573–5583.
 21. Lamy, J., Compin, S. & Lamy, J. N. (1983). Immunological correlates between multiple isolated subunits of *Androctonus australis* and *Limulus polyphemus* hemocyanin: an evolutionary approach. *Arch. Biochem. Biophys.* **223**, 584–603.
 22. Kempter, B., Markl, J., Brenowitz, M., Bonaventura, C. & Bonaventura, J. (1985). Immunological correspondence between arthropod hemocyanin subunits. II. Xiphosuran (*Limulus*) and spider (*Eurypelma, Cupiennius*) hemocyanin. *Biol. Chem. Hoppe Seyler*, **366**, 77–86.
 23. Lamy, J., Bijlholt, M. M. C., Sizaret, P.-Y., Lamy, J. & van Bruggen, E. F. J. (1981). Quaternary structure of scorpion (*Androctonus australis*) hemocyanin. Localization of subunits with immunological methods and electron microscopy. *Biochemistry*, **20**, 1849–1856.
 24. Markl, J., Kempter, B., Linzen, B., Bijlholt, M. M. C. & van Bruggen, E. F. J. (1981). Hemocyanin in spiders, XVI. Subunit topography and a model of the quaternary structure of *Eurypelma* hemocyanin. *Biol. Chem. Hoppe-Seyler*, **362**, 1631–1641.
 25. Sizaret, P.-Y., Frank, J., Lamy, J., Weill, J. & Lamy, J. N. (1982). A refined quaternary structure of *Androctonus australis* hemocyanin. *Eur. J. Biochem.* **127**, 501–506.
 26. Boisset, N., Frank, J., Taveau, J.-C., Billiald, P., Motta, G., Lamy, J. *et al.* (1988). Intramolecular localization of epitopes within an oligomeric protein by immunoelectron microscopy and image processing. *Proteins: Struct. Funct. Genet.* **3**, 161–183.
 27. van Bruggen, E. F. J., Bijlholt, M. M. C., Schutter, W. G., Wichertjes, T., Bonaventura, J., Bonaventura, C. *et al.* (1980). The role of structurally diverse subunits in the assembly of three cheliceratan hemocyanins. *FEBS Letters*, **116**, 207–210.
 28. Markl, J., Decker, H. & Linzen, B. (1982). Hemocyanin in spiders, XV. The role of individual subunits in the assembly of *Eurypelma* hemocyanin. *Biol. Chem. Hoppe-Seyler*, **363**, 73–87.
 29. Voit, R., Feldmaier-Fuchs, G., Schweikardt, T., Decker, H. & Burmester, T. (2000). Complete sequence of the 24-mer hemocyanin of the tarantula *Eurypelma californicum*. *J. Biol. Chem.* **275**, 39339–39344.
 30. Ballweber, P., Markl, J. & Burmester, T. (2002). Complete hemocyanin-subunit sequences of the hunting spider *Cupiennius salei*: recent hemocyanin-remodelling in entelegyne spiders. *J. Biol. Chem.* **277**, 14451–14457.
 31. Averdam, A., Markl, J. & Burmester, T. (2003). Subunit sequences of the 4x6-mer hemocyanin from the golden orb-web spider *Nephila inaurata*: intramolecular evolution of the chelicerate hemocyanin subunits. *Eur. J. Biochem.* **270**, 3432–3439.
 32. van Heel, M. & Frank, J. (1981). Use of multivariate statistics in analysing the images of biological macromolecules. *Ultramicroscopy*, **6**, 187–194.
 33. Lamy, J., Sizaret, P.-Y., Frank, J., Verschoor, A., Feldmann, R. & Bonaventura, J. (1982). Architecture of *Limulus polyphemus* hemocyanin. *Biochemistry*, **21**, 6825–6833.
 34. van Heel, M. & Dube, P. (1994). Quaternary structure of multimeric arthropod hemocyanins. *Micron*, **25**, 387–418.
 35. de Haas, F. & van Bruggen, E. F. J. (1994). The interhexameric contacts in the four-hexameric hemocyanin from the tarantula *Eurypelma californicum*: a tentative mechanism for cooperative behavior. *J. Mol. Biol.* **237**, 464–478.
 36. Hartmann, H. & Decker, H. (2002). All hierarchical levels are involved in conformational transitions of the 4x6-meric tarantula hemocyanin upon oxygenation. *Biochim. Biophys. Acta*, **1601**, 132–137.
 37. Boisset, N., Penczek, P., Taveau, J.-C., Lamy, J., Frank, J. & Lamy, J. (1995). Three-dimensional reconstruction of *Androctonus australis* hemocyanin labelled with a monoclonal Fab fragment. *J. Struct. Biol.* **115**, 16–29.
 38. Taveau, J.-C., Boisset, N., Lamy, J., Lambert, O. & Lamy, J. N. (1997). Three-dimensional reconstruction of *Limulus polyphemus* hemocyanin from cryoelectron microscopy. *J. Mol. Biol.* **266**, 1002–1015.
 39. Meissner, U., Stohr, M., Kusche, K., Burmester, T., Stark, H., Harris, J. R. *et al.* (2003). Quaternary

- structure of the European spiny lobster (*Palinurus elephas*) 1x6-mer hemocyanin from cryoEM and amino acid sequence data. *J. Mol. Biol.* **325**, 99–109.
40. Bijlholt, M. M. C., van Bruggen, E. F. J. & Bonaventura, J. (1979). Dissociation and reassembly of *Limulus polyphemus* hemocyanin. *Eur. J. Biochem.* **95**, 399–405.
41. Brenowitz, M., Bonaventura, C. & Bonaventura, J. (1983). Assembly and calcium-dependent cooperativity of *Limulus* IV hemocyanin: a model system for analysis of structure-function relationships in the absence of subunit heterogeneity. *Biochemistry*, **22**, 4707–4713.
42. Savel-Niemann, A., Markl, J. & Linzen, B. (1988). Hemocyanins in spiders, XXII. Range of allosteric interaction in a four-hexamer hemocyanin: co-operativity and Bohr effect of dissociation intermediates. *J. Mol. Biol.* **204**, 385–395.
43. Brouwer & Serigstad (1989). Allosteric control in *Limulus polyphemus* hemocyanin: functional relevance of interactions between hexamers. *Biochemistry*, **28**, 8819–8827.
44. Adrian, M., Dubochet, J., Lepault, J. & Dowall, A. W. (1984). Cryo-electron microscopy of viruses. *Nature*, **308**, 105–111.
45. van Heel, M., Harauz, G., Orlova, E. V., Schmidt, R. & Schatz, M. (1996). A new generation of IMAGIC image processing system. *J. Struct. Biol.* **116**, 17–24.
46. Chacón, P. & Wriggers, W. (2002). Multi-resolution contour-based fitting of macromolecular structures. *J. Mol. Biol.* **317**, 375–384.
47. Chirgwin, J. M., Przbyla, A. E., MacDonald, R. J. & Rutter, W. J. (1979). Isolation of biologically active ribonucleic acid from sources enriched in ribonuclease. *Biochemistry*, **18**, 5294–5299.
48. Huelsenbeck, J. P. & Ronquist, F. (2001). MRBAYES: Bayesian inference of phylogenetic trees. *Bioinformatics*, **17**, 754–755.
49. Whelan, S. & Goldman, N. (2001). A general empirical model of protein evolution derived from multiple protein families using a maximum-likelihood approach. *Mol. Biol. Evol.* **18**, 691–699.

Edited by R. Huber

(Received 1 September 2006; received in revised form 21 November 2006; accepted 28 November 2006)
Available online 1 December 2006